February 1996 • NREL/TP-411-20708

Amorphous Silicon Research

Annual Subcontract Report
1 October 1994 - 30 September 1995

R. R. Arya, M. Bennett, D. Bradley,
L. Chen, K. Jansen, Y. Li, N. Maley,
J. Newton, C. Poplawski, K. Rajan,
L. Yang
Solarex, A Business Unit of
Amoco/Enron Solar
Newtown, Pennsylvania

National Renewable Energy Laboratory
1617 Cole Boulevard
Golden, Colorado 80401-3393
A national laboratory of the U.S. Department of Energy
Managed by Midwest Research Institute
for the U.S. Department of Energy
under Contract No. DE-AC36-83CH10093

NREL/TP-411-20708 • UC Category: 1262 • DE96000526

Amorphous Silicon Research

Annual Subcontract Report
1 October 1994 – 30 September 1995

R. R. Arya, M. Bennett, D. Bradley,
L. Chen, K. Jansen, Y. Li, N. Maley,
J. Newton, C. Poplawski, K. Rajan,
L. Yang
Solarex, A Business Unit of
Amoco/Enron Solar
Newtown, Pennsylvania

NREL technical monitor: W. Luft

National Renewable Energy Laboratory
1617 Cole Boulevard
Golden, Colorado 80401-3393
A national laboratory of
the U.S. Department of Energy
Managed by Midwest Research Institute
for the U.S. Department of Energy
under contract No. DE-AC36-83CH10093

Prepared under Subcontract No. ZAN-4-13318-01

February 1996

Available to DOE and DOE contractors from:
Office of Scientific and Technical Information (OSTI)
P.O. Box 62
Oak Ridge, TN 37831
Prices available by calling (615) 576-8401

Available to the public from:
National Technical Information Service (NTIS)
U.S. Department of Commerce
5285 Port Royal Road
Springfield, VA 22161
(703) 487-4650

Printed on paper containing at least 50% wastepaper, including 10% postconsumer waste

PREFACE

The work described in this report is the culmination of research performed from October 1, 1994 through September 30, 1995 under Phase I of a subcontract from National Renewable Energy Laboratory to Solarex, a business unit of Amoco/Enron Solar (subcontract number ZAN-4-11318-01). The members of the technical staff at Solarex who participated in the research program have greatly benefited from the interaction and collaboration with other members of the NREL a-Si:H research teams.

EXECUTIVE SUMMARY

Objectives

The principal objective of the research and development program is to accelerate commercialization of low-cost, high-performance, amorphous silicon based multijunction modules. The near term goal of the program is to achieve 12% stable efficiency by 1998 with amorphous silicon multijunction modules.

Approach

The major effort in this program is to develop cost-effective processes which satisfy efficiency, yield and material usage criteria for mass production of amorphous silicon-based multijunction modules. New and improved processes were developed for the component cells and a more robust rear contact was developed for better long-term stability. The efforts in phase I were concentrated on component cells and their incorporation in a-Si/a-SiGe tandem-junction devices and modules.

Status and Accomplishments

- Hydrogen dilution of intrinsic i-layer was explored and a two-step i-layer developed which retains the stability advantages of H-dilution while decreasing the overall deposition time.

- The H-dilution i-layer was optimized to demonstrate a thin-single junction module which degrades only 12% after prolonged light-soaking.

- Improved p-layer deposition was accomplished by combination of low-growth rate and H-dilution. This p-layer has improved reproducibility and results in ease of scale-up to larger areas.

- Developed a manufacturable robust a-Si/a-SiGe tandem-junction process with average initial efficiency of 9.6% and average stabilized efficiency of 8%.

- Demonstrated improvement in light-induced degradation of tandem-junction modules from ~17% to ~15%.

- Demonstrated best tandem-junction module with initial efficiency 10.5% and stabilized efficiency 8.7% with a manufacturable process.

LIST OF FIGURES

LIST OF TABLES

TABLE OF CONTENTS

1.0 Task 1: MID-BANDGAP ALLOY RESEARCH

1.1 Two-Step Hydrogen Dilution in I-layer

H_2-dilution has been demonstrated to be very effective in reducing light induced degradation in terms of defect generation in a-Si:H based alloy materials and as a result solar cell efficiency. As compared to devices made without H_2-dilution, solar cells made with H_2-dilution show much faster and pronounced saturation in efficiency degradation after prolonged light soaking [1,2]. This behavior has significantly boosted the stabilized efficiency of a-Si:H based solar cells. However, one disadvantage of the H_2-dilution technique in depositing the i-layers of solar cells is that it substantially limits the deposition rate. Typically, the deposition rate is 2-5 times faster without the H_2-dilution than with the H_2-dilution. For large scale commercialization, this difference could translate into millions of dollars in capital investment and eventually the cost of the product.

To minimize the impact of H_2-dilution on the deposition rate, we have investigated the use of two-step H_2-dilution in the i-layer deposition. Namely, we limit high H_2-dilution only to a small portion of the i-layer near the p/i interface and use little to no H_2-dilution in the rest of the i-layer. If the stability of an a-Si:H p-i-n solar cell is more dependent on the region near the p/i interface, as many other cell properties are including the overall efficiency, incorporating H_2-dilution only near the interface would capture most of its benefit, but with minimal impact on the average deposition rate. The device structure we used to test this concept is a single junction a-Si:H p-i-n cell in which the first part of the i-layer near the p/i interface is made with normal amount of H_2-dilution and the rest with very little H_2-dilution. While keeping the total i-layer thickness constant, the thickness of the region using high H_2-dilution is varied. These devices with two-step i-layers are then light soaked and compared to solar cells with uniform i-layers made with either the high or the low H_2-dilution as incorporated in the first or the second step of the i-layers, respectively. As shown in Table 1, the initial performance of the devices are quite comparable, except that the one-step cell with low H_2-dilution has somewhat lower V_{oc} and J_{sc} which is partially due to its higher bandgap.

Table 1 Initial performance of solar cells with one- or two- step i-layers

Device #	Device type	V_{oc} (V)	J_{sc} (mA/cm^2)	FF	Eff. (%)
MC5011-1	1-step, high H_2-dilution	0.94	14.4	0.70	9.42
MC5009-1	1-step, low H_2-dilution	0.89	12.6	0.71	8.01
MC5042-3	2-step (500Å/3300Å)	0.93	13.8	0.71	9.14
MC5042-2	2-step (1000Å/2800Å)	0.94	14.6	0.71	9.76

Figure 1 shows the degradation behavior of these cells listed in Table 1 under 1-sun illumination. It is quite expected that the 1-step cell with low H_2-dilution degraded much more than that with high dilution. However, it is very interesting to observe that the two 2-step cells behaved drastically differently. The one with ~1000Å thick H_2-diluted region near the p/i interface had almost the same amount of degradation as the 1-step cell with high H_2-dilution. The other with ~500Å thick H_2-diluted region, on the other hand, degraded about the same amount as the 1-step cell with low H_2-dilution. Therefore, between 500Å and 1000Å lies the transitional thickness beyond which the stability of the 2-step cell is predominantly determined by the i-layer material near the interface.

1.2 Stable Thin Single Junction Modules

In the first phase of the present contract, we have put significant efforts into optimizing the i-layer deposition condition, such as temperature, pressure, power and H_2-dilution ratio for better stabilized first and second junction performance. As a result of these studies, we have recently made a number of 1 ft^2 thin a-Si:H single junction modules. The best module in this group had an initial aperture efficiency of 7.2% and a stabilized efficiency of 6.31% after 1000 hours of AM1.5 light soaking. The total degradation of ~12% in the module efficiency is significantly better than that for similar modules made with the old deposition conditions (~20%). Figure 2 shows the module efficiency as a function of light soaking time.

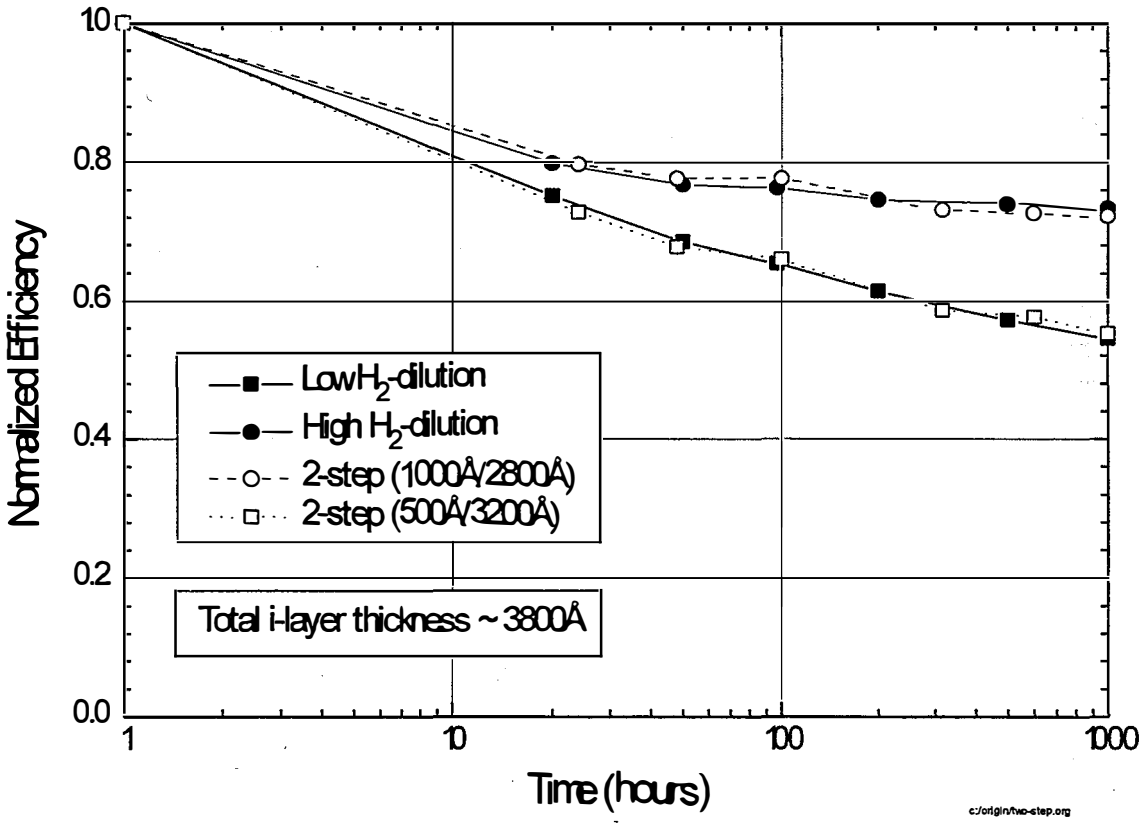

Fig. 1 Degradation of single junction cells made with 2-step i-layers. Data for control cells are also shown for comparison.

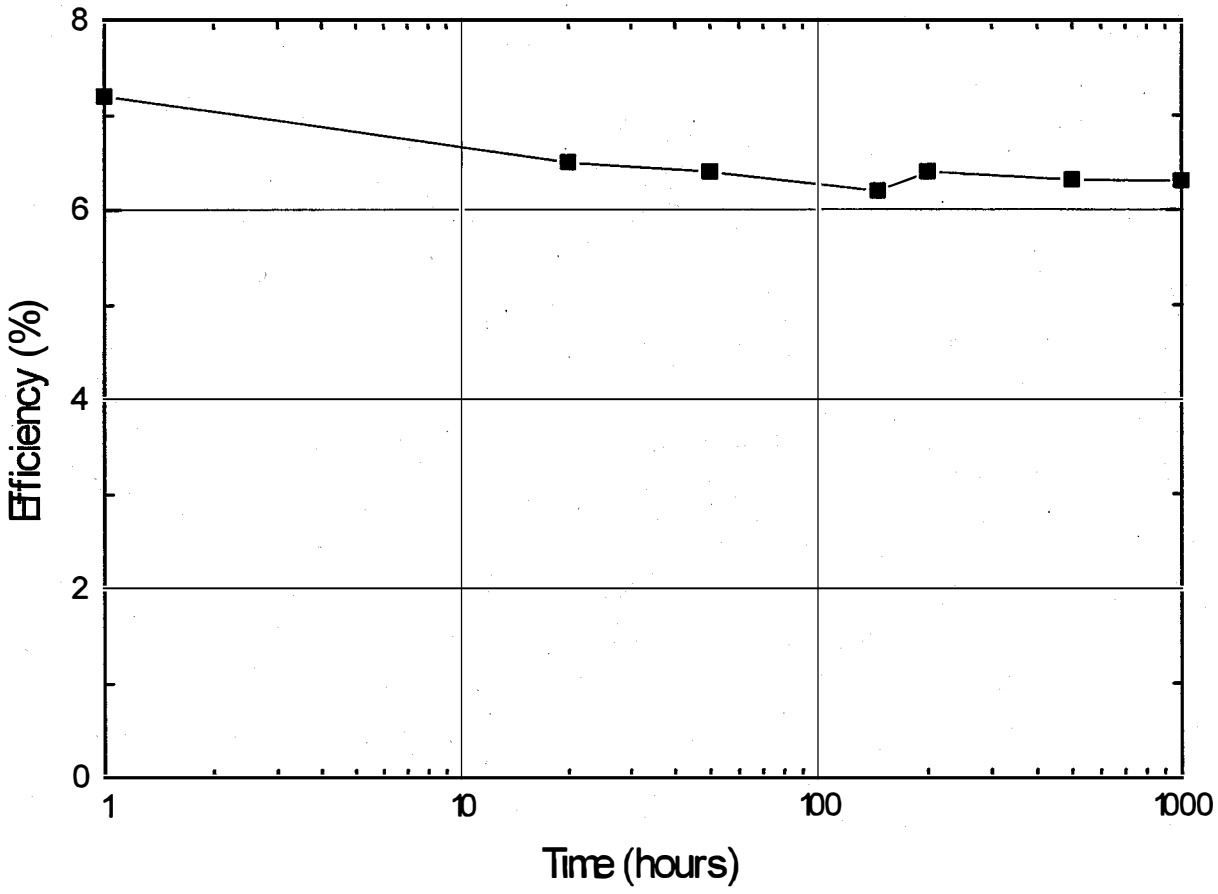

Fig. 2 Efficiency of a thin a-Si:H single junction 1 ft^2 module as a function of light soaking time.

1.3 P_1-layer Optimization

1.3.1 Design-of-experiment Approach

Optimizing the SnO_2/p_1-SiC interface and the p_1 layer is extremely important both for improving device efficiency and for scaling up the Si deposition process to make large area modules. This task is further complicated by the fact that the p_1-layer is very thin (~100 Å), and requires the use of SiH_4, CH_4, TMB or diborane, and sometimes a carrier gas for the dopant. The parameter space for p_1-layer depositions is very large due to the number of parameters involved - number of gases, their flow rates, pressure, discharge parameters, and deposition time, to name a few - and the interaction between the parameters. Uniformity over large areas and run-to-run reproducibility are also issues that affect module performance and hence the conclusions one can draw from process optimization experiments. In situations such as these, design-of-experiments is an very powerful tool for process optimization. A well-designed and randomized design-of-experiments study enables us to (i) identify parts of the parameter space that should be further explored and (ii) understand interaction between different parameters, with a minimum number of experiments.

We have developed a standard p_1-layer which has enabled us to demonstrate 8 % stable efficiency on 4 ft^2 tandem modules with the following typical stabilized photovoltaic parameters: V_{oc} = 1.49V, J_{sc} = 9.8 mA/cm^2, and FF = 0.64 [3]. In order to further improve the p_1-layer we have recently carried out a design-of-experiments study involving four variables: (i) total gas pressure, (ii) discharge current, (iii) CH_4/SiH_4 ratio, and (iv) dopant/SiH_4 ratio. There were two objectives: (i) to determine the robustness of the standard process, and (ii) to determine if efficiency can be improved while maintaining or improving process control. This study was carried out using our standard 4 ft^2 Si/SiGe tandem as the test structure. All the layers with the exception of p_1 were same for all the modules. For the four parameters listed above values 10-40 % higher and lower than the standard were examined. In all, 12 standard modules and 32 modules with different p_1-layers were made, and 42 of the 44 modules were tested.

A detailed analysis of the results showed that within the 95 % confidence interval discharge current and dopant/SiH_4 ratio did not affect the module performance. Total pressure and CH_4/SiH_4 ratio, on the other hand, were important. Table 2 summarizes the results.

From the table we can see that first three groups of modules yield results that are identical to the standard (Group 5), while Group 4 has 1-3 % higher efficiency and also lower variance. Further analysis of the data shows that this improvement is primarily due to a more transparent p_1-layer which results in higher J_{sc}. Though this 1-3 % gain is relatively small, it is quite significant, and it can be easily implemented into a production process. We will also be examining if additional gains in efficiency are possible through further optimization of pressure and CH_4/SiH_4 ratio. This experiment clearly demonstrates the usefulness of the design-of-experiments approach when seeking small gains by optimizing processes with several parameters.

Table 2 Results of design-of-experiments study for p_1-layer optimization on 4 ft^2 Si/SiGe tandem-junction modules

Group	Total Pressure	CH_4/SiH_4 ratio	# of modules	mean η and 95% confidence interval*
1	Low	Low	8	8.88 +/- 0.08
2	Low	High	6	8.93 +/- 0.07
3	High	Low	8	8.97 +/- 0.07
4	High	High	8	9.18 +/- 0.02
5	Standard	Standard	12	8.96 +/- 0.08

* Initial efficiency measured at Solarex. NREL measurements are ~ 6% higher.

1.3.2 P-layer Made at Low Growth Rate

We have explored the use of p-layer made at relatively low growth rate, primarily due to concerns about the poor controllability of the standard p-layer. The total deposition time for the standard p-layer is less than 20 sec, making it sensitive to the initial plasma ignition condition which is not well controlled. Longer deposition time in p-layer deposition will certainly reduce such sensitivity and hence improve the process reproducibility. While the benefit of the low growth rate p-layer in these areas has not yet been fully tested, additional benefit to the device performance, to our surprise, has been observed. As shown in Table 3, V_{oc} and J_{sc} are higher in devices made with low growth rate p-layer as compared to those with standard p-layer. It should be noted that the relatively low V_{oc} in the case of standard p-layer is normal for the type of single junction devices used here.

Table 3 Single junction a-Si:H devices with standard or low growth rate p-layer

Sample #	P-layer	V_{oc} (V)	J_{sc} (mA/cm^2)	FF	η	QE_{400nm}
MC5043-2	standard	0.86	13.3	0.72	8.16	0.59
MC5051-1	standard	0.87	13.5	0.72	8.46	0.55
MC5055-2	low growth rate	0.89	14.0	0.74	9.18	0.59
MC5058-2	low growth rate	0.89	13.9	0.73	9.03	0.62
MC5058-3	low growth rate	0.90	13.6	0.74	9.07	0.58

SiO_x P-layer

We have briefly tested a-SiO_X:H *p*-layers using N_2O as the feedstock for oxygen to widen the optical bandgap of a-Si:H. Such a *p*-layer has been shown to be superior to the conventional a-SiC:H by the Fuji group [4]. Good V_{oc} and FF were observed in single junction a-Si:H *p-i-n* cells, however the J_{sc} was relatively low in all cases of varying N_2O content in the feed-gas mixture. The blue response was severely suppressed (showing strong electrical bias dependence in QE). This may be due, in part, to the incompatibility of the a-SiO_X:H *p*-layer and the a-Si:H *i*-layer. Further work is needed to identify optimum deposition conditions for such a *p*-layer using N_2O as the oxygen feedstock instead of CO_2 as proposed by the Fuji group.

1.4 The Degradation of Amorphous Silicon Solar Cells at Elevated Temperatures

1.4.1 Introduction

Earlier work [5] had shown that commercial amorphous silicon (a-Si:H) solar cells degrade at elevated temperatures ($\geq 150^0$C) due to the interdiffusion of aluminum and silicon at the rear contacts. More recently, Solarex has developed a-Si:H solar cells that utilize textured tin oxide as a front contact and zinc oxide/aluminum as a rear contact [6].

The purpose of this study was to investigate the degradation of this new device structure at elevated temperatures and also when exposed to intense illumination at elevated temperatures. We were particularly interested in whether the degradation mechanisms observed at elevated temperatures could play a role in limiting the lifetime of the a-Si:H solar cells under normal operating conditions.

1.4.2 Experimental Conditions

The a-Si:H solar cells were either single-junction p-i-n cells or a-Si:H/a-SiGe:H tandem cells that were fabricated using tin oxide coated glass substrates and zinc oxide/aluminum rear contacts. The tin oxide was deposited on soda-lime-silicate glass using atmospheric CVD. The amorphous alloy layers were deposited using plasma-enhanced chemical vapor deposition (PECVD) at substrate temperatures in the range of 200-260^{0}C. The zinc oxide was deposited using low-pressure CVD, and the aluminum was magnetron sputtered on top of the zinc oxide.

Most of the cells were heat treated in air at temperatures ranging from room temperature to 260^{0}C; a few cells were heat treated in vacuum (~ 10^{-3} Torr) and exhibited similar degradation. Some cells were exposed to intense illumination (~50 suns) from a xenon arc lamp for various times and temperatures.

1.4.3 Results

In one series of experiments, tandem cells (deposited at 200^{0}C) were heated at various temperatures for one hour in the dark in air. As shown in Fig. 3, the cells exhibit a slight improvement in performance after being heat treated for one hour at 180^{0}C due to an improvement in the zinc oxide/aluminum rear contact. However, after heat treating the cells at higher temperatures, the performance of the solar cells starts to degrade. The onset of this thermal degradation depends on the deposition conditions and moves to higher temperatures for junctions deposited at higher substrate temperatures [7].

When exposed to ~50 suns for 1 hour at 50^{0}C, the cells degrade by ~ 17% due to the creation of metastable defects [8]. As shown in Fig. 3, this light-induced degradation can be reversed by heat treating the cells for 1 hour at 180^{0}C and can also be suppressed by imposing a reverse bias of -6V. When the exposure temperature is increased to 130^{0}C, the amount of light-enhanced degradation is reduced due to annealing effects. However, the light-induced degradation increases again for higher exposure temperatures, and as shown in Fig. 3, the light-induced degradation at elevated temperatures is significantly increased over that observed for cells heat treated in the dark. This light-enhanced degradation at elevated temperatures is irreversible, and as also shown in Fig. 3, is further increased by the application of a reverse bias field.

Fig. 4 shows spectral response data for a single-junction p-i-n cell that was heat treated for various times at 220^{0}C in the dark. Most of the degradation is observed to occur in the short-wavelength regime. This behavior is different than that observed for cells exposed to intense illumination at lower temperatures (~ 50^{0}C) where the degradation in the spectral response occurs mainly in the long-wavelength regime.

Application of a strong reverse bias to a p-i-n or to a tandem cell at elevated temperatures in the dark causes a slight decrease in the amount of degradation. This effect is seen in the spectral response data of Fig. 5 where three identical p-i-n cells were heat treated in the dark at 260^{0}C with (a) no bias, (b) -10 V reverse bias and (c) a forward bias that produced a current density of about 500 mA/cm^2. As shown, the reverse bias tends to suppress the degradation in the dark while the forward bias enhances the degradation significantly as is also observed when the cells are exposed to intense illumination (~ 50 suns) at elevated temperatures.

The increased degradation of either single-junction or tandem cells that are exposed to intense illumination at elevated temperatures occurs mainly in the short wavelength regime of the spectral response. When a strong reverse bias is applied to a p-i-n cell under intense illumination at elevated temperatures, the degradation in the spectral response in short wavelength regime is increased even more as shown in Fig. 6. This behavior is also different from that observed for cells exposed to intense illumination at lower temperatures where a strong reverse bias suppresses the light-induced degradation (see Fig. 3).

When a strong reverse bias is applied to a tandem cell under intense illumination at elevated temperatures, the spectral response data shows that the degradation is accelerated in both junctions (see Fig. 7). Moreover, this further acceleration of the light-enhanced degradation is

observed to occur primarily in the vicinity of the p/i interfaces of both junctions. The data represented by solid diamonds and solid triangles in Fig. 7 show the contributions of the front and rear junctions to the overall spectral response after the 50 suns exposure at 220^0C. The data represented by open triangles and open diamonds show the additional decrease in quantum efficiencies of the front and rear junctions when a reverse bias of - 6 V is applied to an identical device exposed to 50 suns for 1 hour at 220^0C.

In order to study the kinetics of the degradation at elevated temperatures, a characteristic decay time was defined by determining how long it took for the quantum efficiency at 420 nm to decrease by 25%. The decay times for p-i-n cells heat treated in the dark at various temperatures are plotted on a semi-logarithmic scale as a function of 1000/T in Fig. 8. Decay time data for similar p-i-n cells that were exposed to intense illumination is also shown in Fig. 8.

1.4.4 Discussion

The degradation at elevated temperatures is not associated with the diffusion of impurities from the p-layer or the substrate since similar effects are observed in Shottky barrier cells and in the back junction of tandem cells.

An analysis of the decay time data shown in Fig. 8 indicates an activation energy of about 1.7 eV for cells heat treated in the dark and about 1.0 eV for cells heat treated while exposed to intense illumination. These activation energies are close to those measured for hydrogen diffusion in the dark [9] and under intense illumination [10].

The experimental results can be largely explained by assuming that hydrogen is diffusing out of the a-Si:H in the vicinity of the p-layer at elevated temperatures. This is expected since the diffusion of hydrogen is significantly larger in p-type material than in intrinsic or n-type material [11] so the degradation would occur mainly near the p/i interface as observed. Moreover, the diffusion of hydrogen in a-Si:H increases significantly when the material is exposed to intense illumination [12] so that the degradation at elevated temperatures would be light-enhanced as observed.

Since the diffusion of hydrogen is reduced when a reverse bias is applied [13], the degradation of p-i-n cells in the dark at elevated temperatures is reduced by the application of a reverse bias as shown in Fig. 5. The application of a forward bias in the dark increases the degradation at elevated temperatures due to the injection of carriers as in the case of exposure to intense illumination.

The increased degradation that is observed when cells under intense illumination at elevated temperatures are subjected to a strong reverse bias may be interpreted in terms of hydrogen ion motion. For the p-i-n cells used in the present study, the increased degradation in the short-wavelength spectral response suggests that protons may be driven by the field toward the tin oxide/p-layer interface.

Several observations strongly support this hypothesis. First, the tin oxide electrode darkens appreciably when the devices are exposed to both intense illumination and a large reverse bias at elevated temperatures (darkening is not observed in the absence of a reverse bias). This observation implies that field-driven protons are reducing the tin oxide at the interface. Moreover, in some cases, small blisters are evident in the electrode region and may be due to the generation of water vapor and the local accumulation of hydrogen gas molecules. Finally, SIMS data show a decrease in the hydrogen concentration in the vicinity of the p/i and the n/i interfaces after exposure to 50 suns illumination at 220^0C for 8 hours.

Recent experiments with n-i-p cells indicate that negative hydrogen ions may also be moving in a-Si:H when the cells are exposed to intense illumination at elevated temperatures. Discoloration of the tin oxide electrodes is also observed for n-i-p cells when subjected to a strong reverse bias at elevated temperatures in the presence of intense illumination, but the effect is less pronounced than that observed for p-i-n cells.

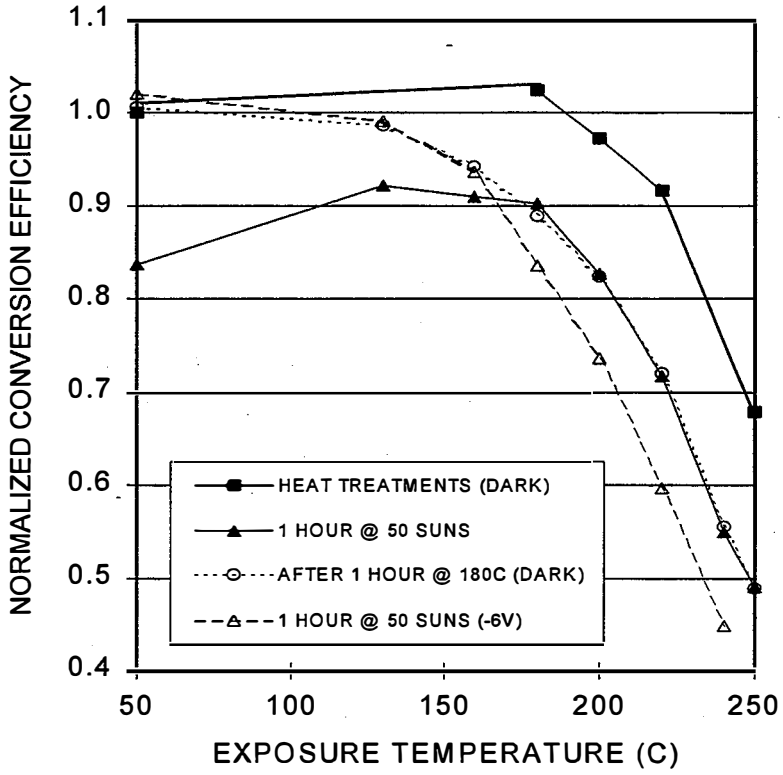

Figure 3 The normalized conversion efficiency as a function of exposure temperature for tandem cells.

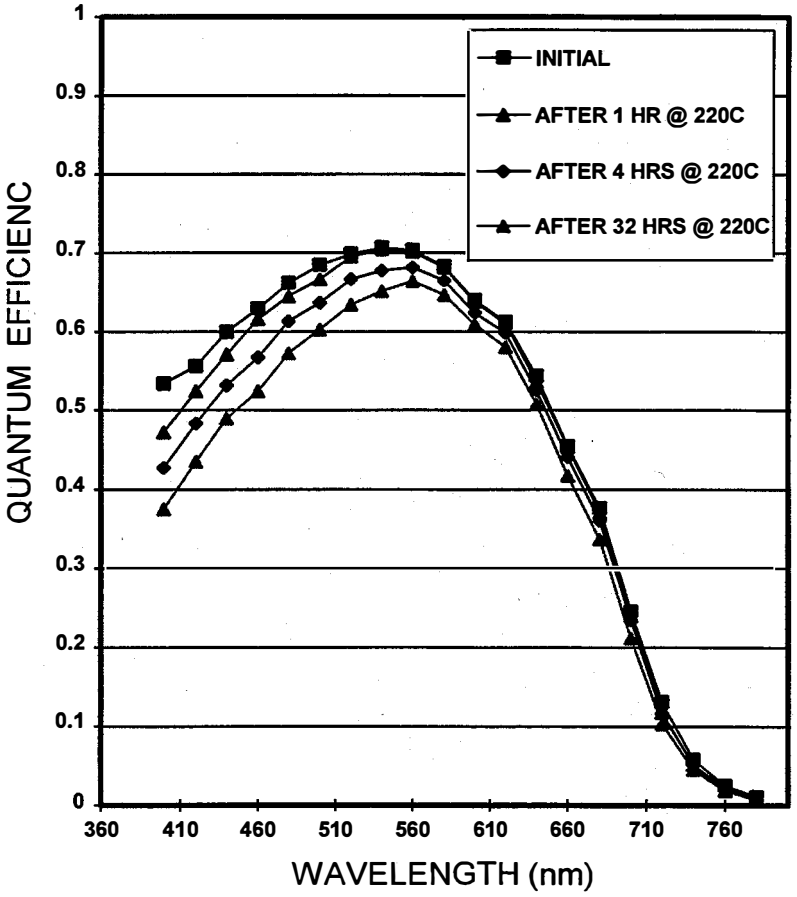

Figure 4 The spectral response for a p-i-n cell heat treated in the dark.

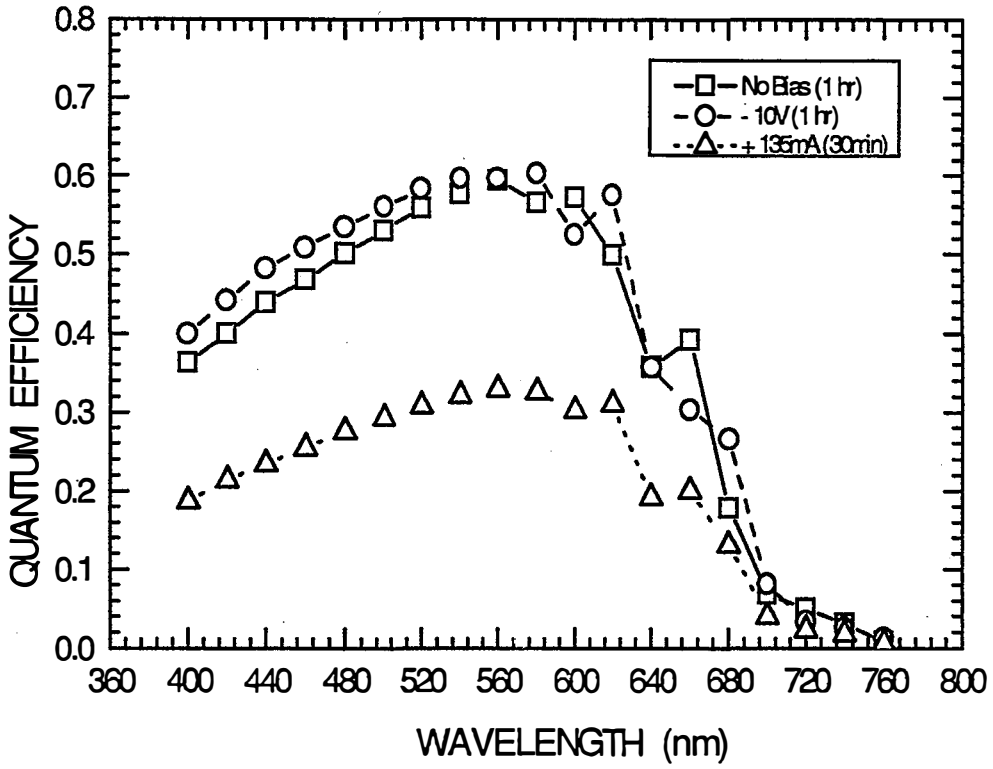

Figure 5 Spectral response data for three identical p-i-n cells subjected to different bias conditions at 260°C in the dark.

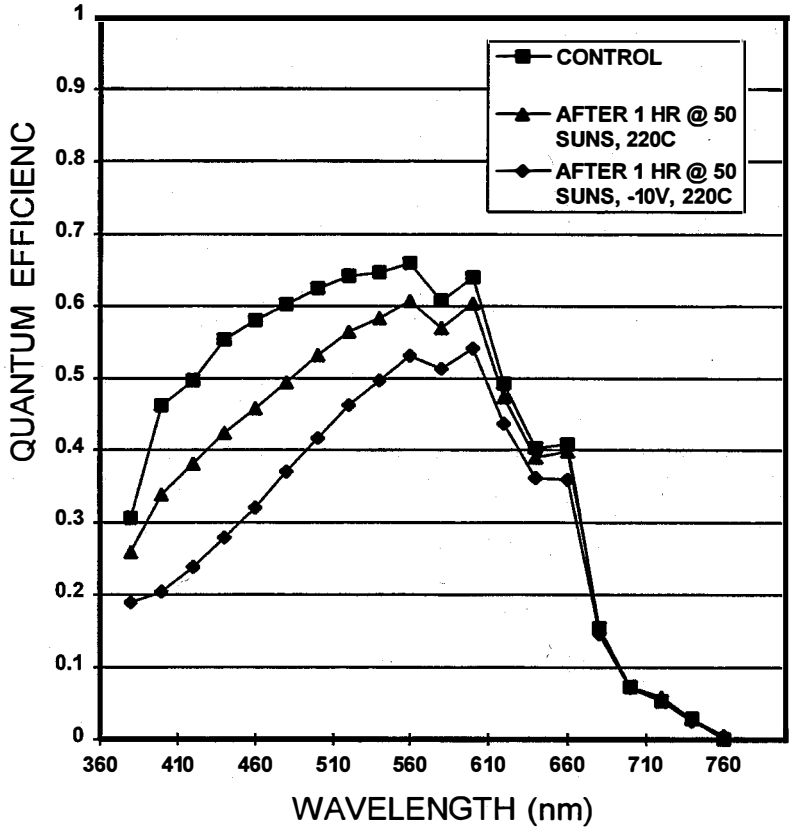

Figure 6 Spectral response data for three identical p-i-n cells where one was a control and two cells were subjected to different bias conditions at 220^0C under 50 suns illumination.

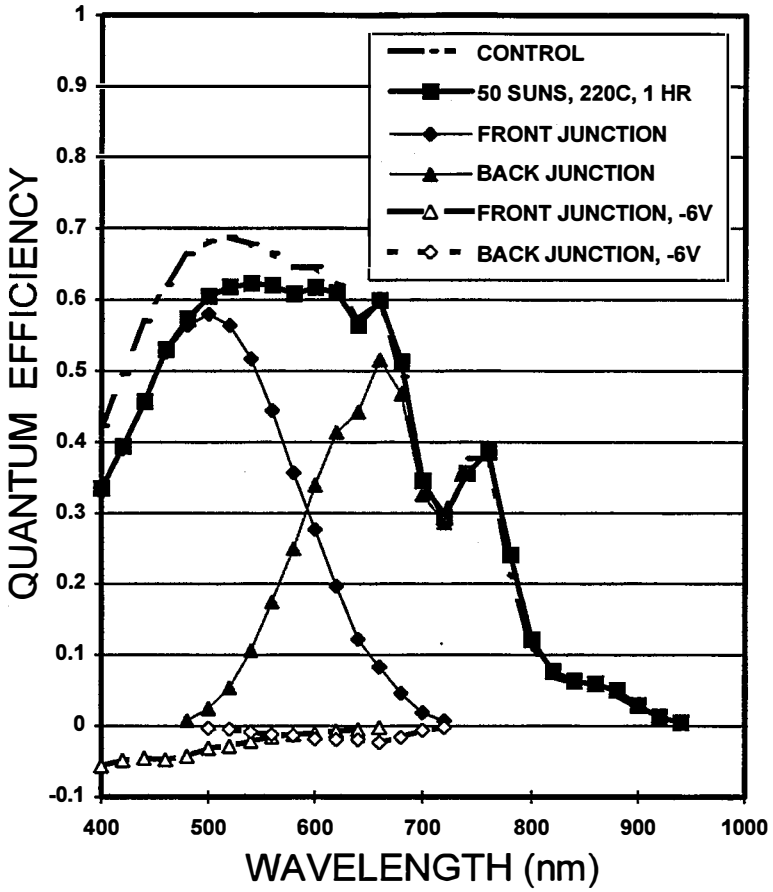

Figure 7 Spectral response data for three identical tandem solar cells where one cell was a control and two cells were subjected to different bias conditions at 220°C under 50 suns illumination.

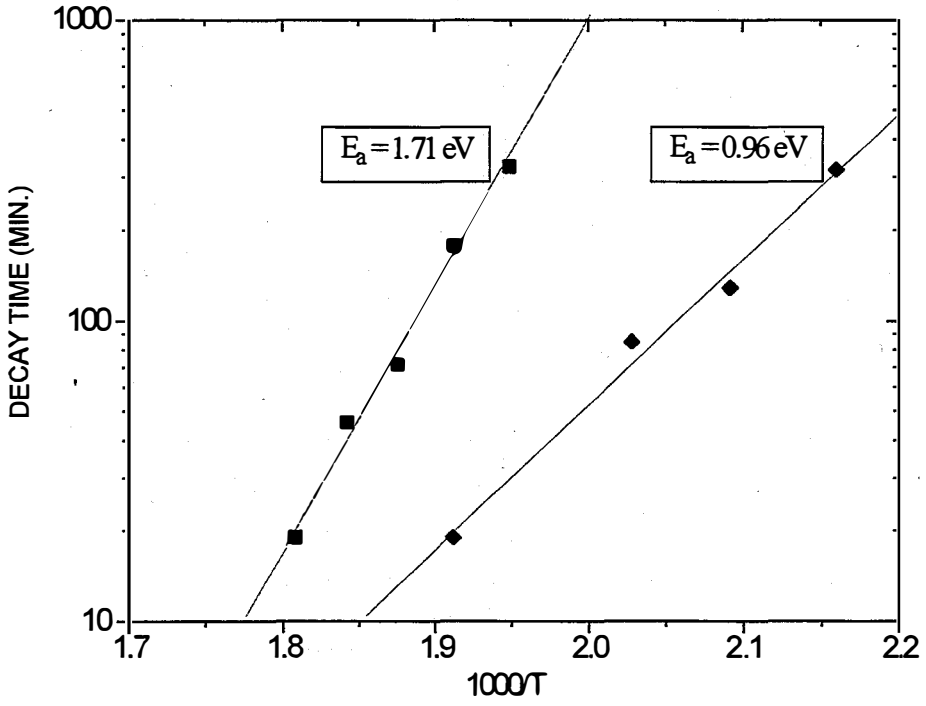

Figure 8 Decay time data for p-i-n cells heat treated in the dark (squares) and under 50 suns illumination (diamonds).

1.5 Identification of Fast and Slow Defects by Electroluminescence Spectroscopy

1.5.1 Introduction

We have recently collaborated with D. Han at University of North Carolina in using electroluminescence spectroscopy (EL) to characterize the "fast" and "slow" defects which were first identified in the kinetic study of photo-degradation of solar cells [14]. The time constants for these two types of defects in both generation and annihilation processes are different by about a factor of 10. Further more, we found that while "fast" and "slow" defects co-exist in solar cells made with pure silane, cells made with H_2-dilution appear to have predominantly the "fast" defects only, resulting in much faster saturation of photo-degradation [15]. Studying the same cells made with and without H_2-dilution using EL spectroscopy, we attempt to further distinguish the two defects in terms of their energy distribution and measure their photodegradation kinetics directly.

1.5.2 Results and Discussion

The EL spectrum of a-Si:H is typically characterized by two bands [16]: the main-band centered at ~1.2 eV is due to tail-to-tail radiative recombination, and the defect-band centered around 0.9 eV is due to defect-to-tail radiative recombination. Since the EL spectrum line shape depends upon the applied field and the measurement temperature [17,18], in this study we compare EL spectra measured under the same applied voltage and at the same temperature.

Figure 9 shows the EL spectra for both types of cells at 90 K. It is well known that at low temperatures ($T < 100$ K) the dominant recombination mechanisms in a-Si:H are the radiative transition between band tail states and the non-radiative transition from the band edge to the defect states (silicon dangling bonds). The radiative transition from the band tail to the defects, on the other hand, is much (2-3 orders of magnitude) weaker. Therefore, one can see that in Fig. 9 the 1.2 eV main-band emission dominates in both cells. The subtle line shape differences between the two types of cells in the EL main-band emission are likely due to small differences in the bandgap (<0.1 eV) and the tail states distribution of the two i-layer materials.

As temperature increases, the excited carriers are no longer trapped in the tail states and therefore the tail-to-tail recombination is substantially quenched by the tail-to-defect recombination. As a result, the EL defect-band is relatively enhanced and becomes dominant at room temperature. Figure 10 shows the EL spectra for the same group of cells as in Fig. 9 measured at 300 K with 0.8 V bias voltage. We observed that the defect band for the cell made with H_2-dilution is dominated by a single peak at ~0.9 eV and that for the cell made without H_2-dilution has a much more pronounced second peak at ~0.75 eV. Even though the line shape at the low energy side of the 0.75 eV peak is slightly affected by the cut-off energy of the Ge detector, the double-peak feature in the non-diluted cell is clear.

Since the defect band luminescence provides direct information on the defect electronic structure of the material including its density as well as energy distribution, it is very interesting to study the evolution of the defect properties as the material is being light soaked. We have exposed

both types of cells to 200 mW/cm^2 white light through the p-layer. The light soaking condition used was similar to the performance photodegradation studies of the same types of solar cells. The EL spectra were measured at various stages of light soaking such as those shown in Fig. 11 for samples made without H_2-dilution. As the solar cells are being light soaked, the intensity of the EL main band (1.0-1.4 eV) decreases and that of the defect-band increases due to the increase of the density of defect states. To investigate the creation kinetics for individual components in the defect band, we have analyzed the intensities of the two peaks at ~0.9 eV and ~0.75 eV, respectively. The results are plotted in Figs. 12a and 12b for cells made with and without H_2-dilution, respectively. As shown in Fig. 12a, the intensity of the dominant peak at 0.9 eV for the H_2-diluted cell increases first, but rapidly stabilizes after only ~10 hours of light soaking. No significant change in the low-energy shoulder can be resolved for this type of device. In contrast, for the non-diluted cell as shown in Fig. 12b the peak at 0.75 eV is much more pronounced and the intensity for both components increases significantly with light soaking. More interestingly, while the 0.9 eV peak also stabilizes after 10-100 hours of light soaking, the 0.75 eV peak continues to rise and no sign of saturation is seen even beyond 1000 hours of light soaking. These observations for both types of cells could be entirely consistent with the results of the solar cell degradation studies [14,15], if we assume that the 0.9 eV and 0.75 eV peaks in the defect band are associated respectively with the "fast" and "slow" defects identified from cell degradation kinetics. Thus, the electroluminescence measurements have not only confirmed the existence of the two kinetically different defect states in certain a-Si:H, depending on the deposition condition, but also provided their unique energy characteristics in the electronic energy bandgap.

Now we know the kinetic as well as energy characteristics of the two light induced defect components which may or may not co-exist in the material, one would probably question next what are the structural origins of these defect states and the mechanisms by which they are created or annihilated. Previous calculation of the dangling bond relaxation energies showed that strong electron-phonon coupling at the dangling bond defects can shift the defect energy level as much as 0.2-0.3 eV [19]. On the other hand, tight-binding calculation showed [20] that neighboring impurity atom such as oxygen can also cause a shift in the DB energy level with a similar magnitude. These are some of the possibilities to be considered in further investigating the correlation between a particular type of defect state with certain microstructure.

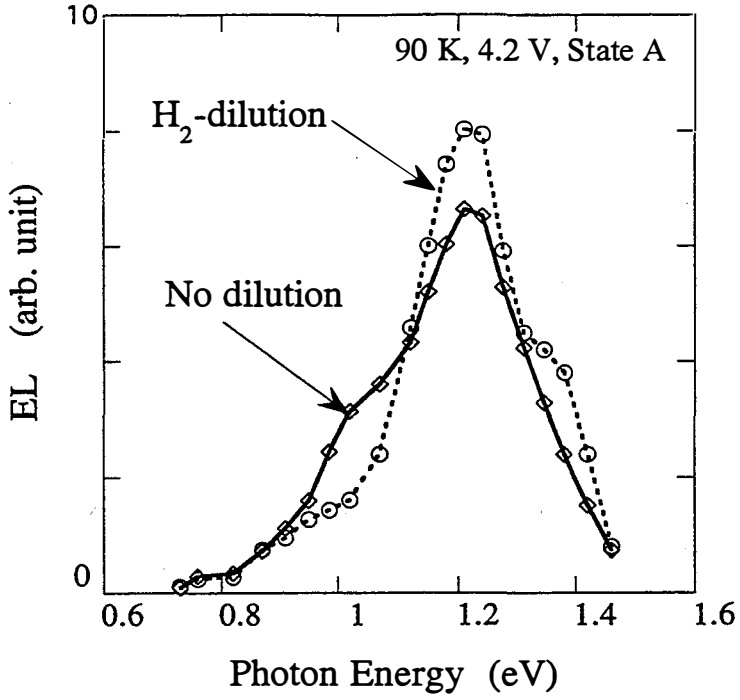

Fig. 9 EL spectra of a-Si:H p-i-n solar cells made with and without H-dilution under 4.2 V at 90 K. Both cells were in the initial state (State A).

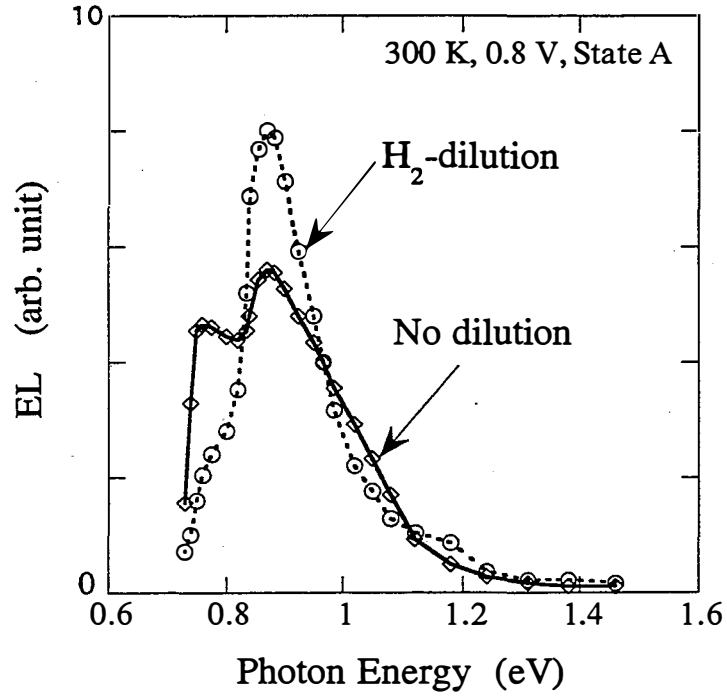

Fig. 10 EL spectra of a-Si:H p-i-n solar cells made with and without H-dilution under 0.8 V at 300 K. Both cells were in the initial state (State A).

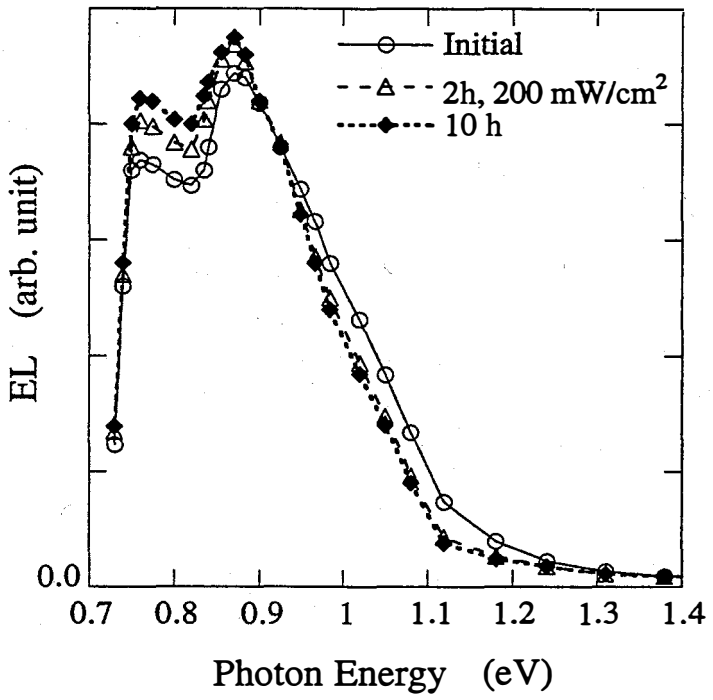

Fig. 11 EL spectra of cells made without H_2-dilution under 0.8 V at 300 K at various stages of light soaking.

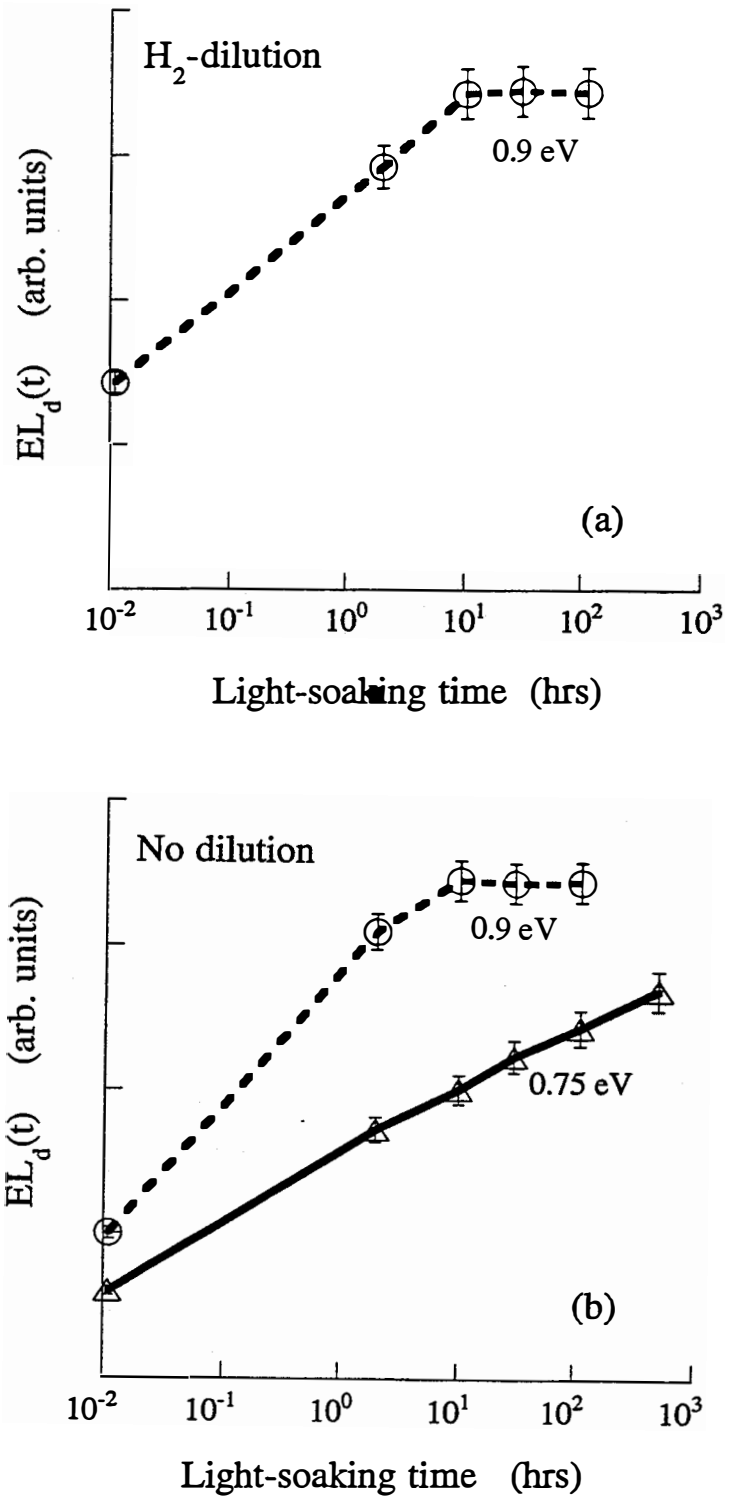

Fig. 12 EL intensities of defect components at ~0.9 eV and ~0.75 eV as a function of light-soaking time for (a) cells made with H_2 dilution and (b) without dilution.

2.0 Task 2: LOW-BANDGAP ALLOY MATERIALS

2.1 Optimization of SiGe Back Junction

We have been in pilot production for a-Si:H/a-SiGe:H tandem (double junction) modules for over a year. The standard device structure run on the pilot line has a relatively low bandgap (~1.45 eV) and thick a-SiGe:H i-layer in the back junction which generates about 20 mA/cm^2 total current with ZnO/Al rear contact. The average degradation of such modules after ~1 000 hours of one-sun light soaking has been established to be ~17% which has been confirmed by the recent NREL indoor light soaking study (see section **4.5.2**).

Based on our experience with single junction devices which show a broad maximum for the stabilized module efficiency as a function of i-layer thickness, it was proposed that the stability of tandem devices could also be significantly improved by reducing the thickness of both i-layers. Thus, we have started evaluating two approaches to reducing overall device thickness. The first is to reduce thickness of both i-layers without changing much of the bandgap of the a-SiGe:H i-layer, and the second is to reduce only the thickness of the front junction i-layer but balance the junctions mostly by reducing the Ge content in the i_2-layer. In addition to performance advantages, both approaches lead to substantial increase in production throughput (decrease in deposition time) and great reduction in raw material consumption, especially the costly GeH_4.

While we expect a significant reduction in the light induced degradation of the thin tandem cell structure, we also found that the initial efficiency of thin tandem cells to be comparable to the standard tandem devices. As shown in Table 4 where the average parameters of a large number of standard and the thin tandem solar cells (~0.2 cm^2) are compared, the loss in J_{sc} for the thin tandem module is well compensated by the gain in FF and V_{oc}. Figure 13 shows the QE of both types of tandem cells. The total current of the thin tandem cell is about 4% lower than that of the standard cell.

Table 4 Average initial parameters for the standard and thin tandem solar cells

Type	V_{oc} (V)	FF (%)	J_{sc} (mA/cm^2)	Eff. (%)
Standard	1.52	67.5	9.71	9.97
Thin	1.54	69.8	9.36	10.06

Preliminary degradation data on thin tandem solar cells confirmed our expectation that these devices degrade significantly less than the thicker standard tandem cells. Figure 14 shows the normalized efficiency of thin tandem cell as a function of light soaking time. After 600 hours of continuous light soaking at 50°C, the cell only lost ~10% of its initial performance as compared to typically ~15% loss for cells made with the standard process.

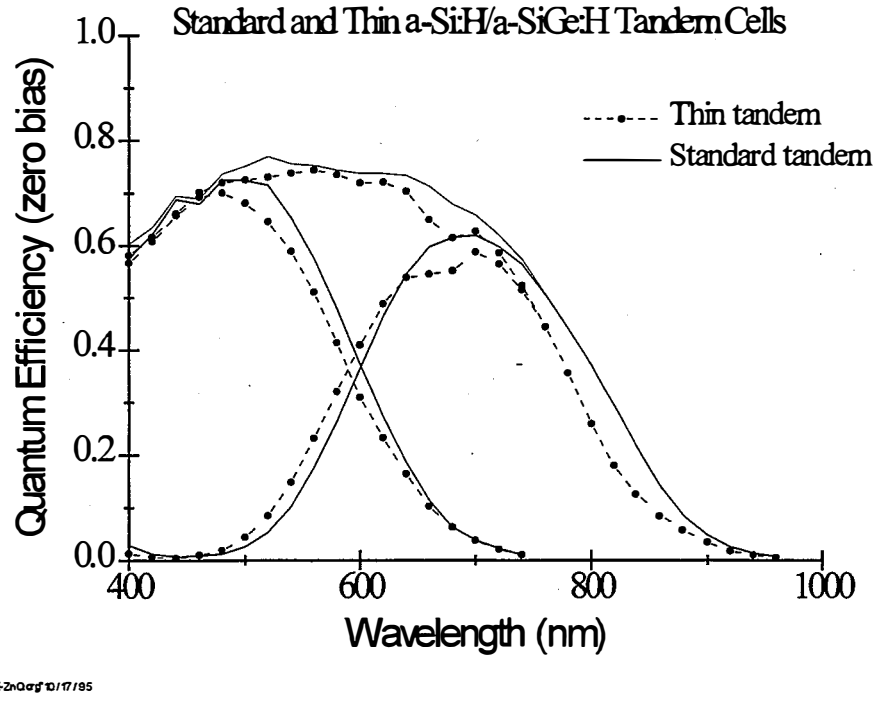

Figure 13 QE of thin and standard tandem devices.

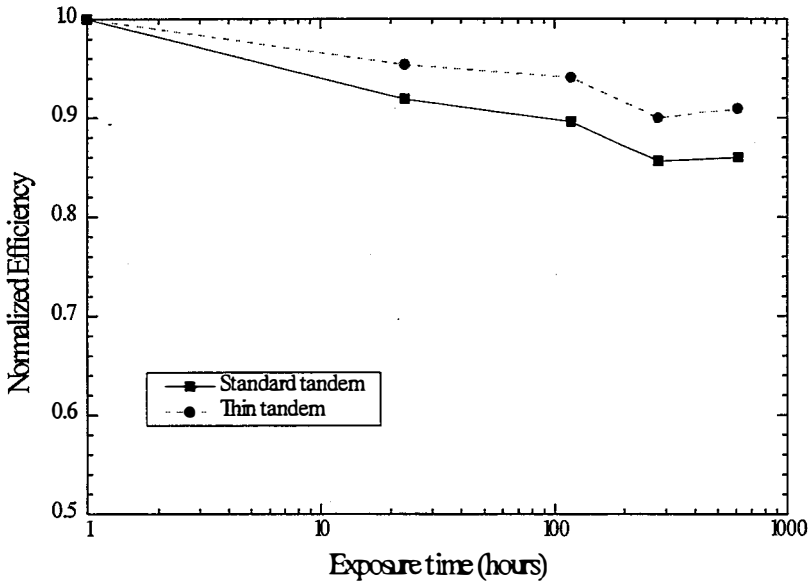

Figure 14 Degradation of thin and standard tandem cells as a function of exposure time.

2.2 Hot Wire/PECVD System for Low Bandgap Alloys

We recently modified a deposition system so that it could run in either a hot wire or a plasma-enhanced CVD mode or in a combination of the two modes. A schematic diagram of the system is shown in Fig. 15. Two DC power supplies are used to control the potential between the substrate and the grids and are isolated from the AC lines that are used to heat the hot wire grid. The hot wire grid is actually an array of 11 parallel, coiled tantalum wires that covers an area of about 90 cm^2, and the system is configured so that the substrate can be heated independently.
The first films were deposited using just the hot wire mode. A deposition rate of about 7.5 Å/s was obtained when the hot wire grid was heated with about 1.3 kW of AC power. The resulting films were relatively uniform over the entire 3" X 3" substrate area. The substrate temperature was ~ 500^0C due to heating from the hot wire grid alone. The system is being modified to allow cooling of the substrate so as to gain more control over the deposition conditions.

We recently deposited some a-Si:H films using the DC triode mode and obtained good uniformity over the entire substrate. Preliminary results indicate that both the deposition rate and the feedstock material utilization can be significantly improved over the normal DC anodic diode mode.

After completing an evaluation of the DC triode mode, we plan to progress to an exploration of the film properties using both the hot wire and DC triode mode simultaneously.

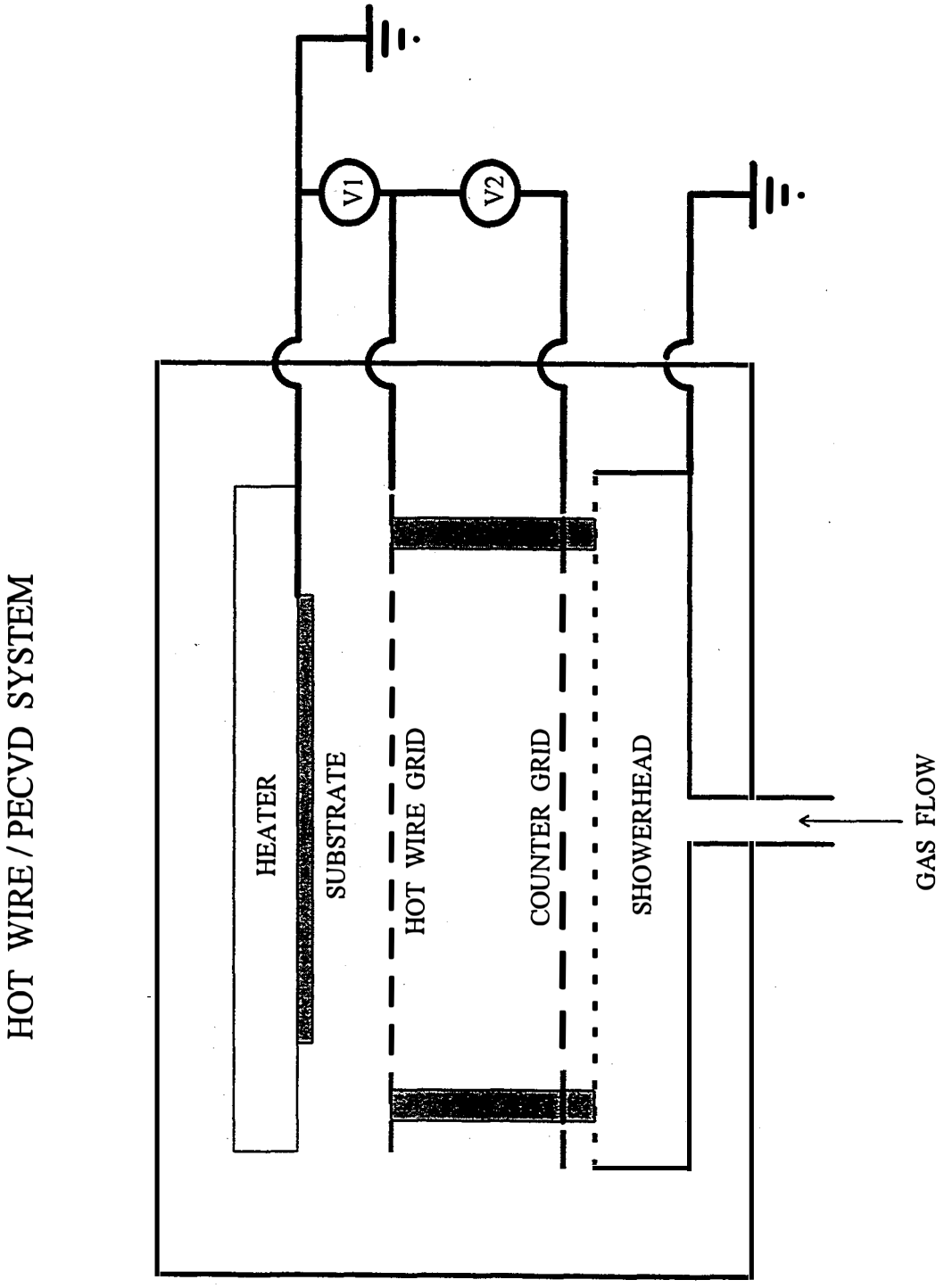

Figure 15 A schematic diagram of the hot wire/PECVD system.

3.0 Task 3: MULTIJUNCTION DEVICES AND MODULES

3.1 ZnO Front Contact

It has long been recognized that ZnO is potentially a much more superior TCO material than SnO_2 as a front contact. It is intrinsically more transparent than SnO_2 resulting in as much as 10% increase in J_{sc} for a-Si:H based multijunction solar cells. Depositing ZnO using a LPCVD process of diethylzinc with H_2O and a dopant such as B_2H_6 at a substrate temperature <200°C adds additional advantages over APCVD SnO_2 in controllability and ease of manufacturing. However, difficulties do exist in incorporating ZnO into modules: (1) there is a contact barrier at the ZnO/SiC p-layer interface which causes lower FF and Voc if the same p-layer is used, (2) it is difficult to scribe ZnO cleanly and reliably by laser, (3) cleaning is also more difficult because ZnO is softer and under certain conditions soluble in water.

We have optimized ZnO and the p-layer deposition conditions to maximize gain in J_{sc} to 6-10% and minimize loss in V_{oc} and FF due to contact barrier to <2%. Figure 16 shows the J-V curve and the quantum efficiency of a typical a-Si:H/a-SiGe:H tandem solar cell made on a textured ZnO substrate.

We have done several experiments to make 1 ft^2 modules using ZnO front contact. We can reproducibly make uniform 1 ft^2 ZnO front contact samples with >82 % transmission, 15 % haze, and 15 Ω/square sheet resistance. However, in comparison with SnO_2, we observe a larger loss in efficiency when we scale up from ZnO cells to modules. Initially we suspected that this problem was entirely due to the ZnO front contact scribe. More recently we have found that the metal scribe is also contributing to the module performance loss.

Looking at the scribes under the microscope it is apparent that the interaction between the film and the laser beam is quite different for the two materials. For ZnO there is a wider region adjacent to the scribe that is adversely affected by the scribing process. SEM micrographs show that this region is substantially rougher than the rest of the film. We suspect that Si coverage over these rough regions is not very conformal, leading to a greater degree of shunting across the cells. We explored the parameter space for the front contact scribing process and identified conditions that yield cleaner scribes. However, even under optimal conditions the scribes are not as clean as they are on SnO_2. New approaches for laser scribing ZnO are being explored and results will be reported later.

The metal scribe is also contributing to the module performance loss. We verified this by the following experiment: We made several small area cells (0.25 cm^2) using ZnO and SnO_2 as the front contact. We quantified the degree of shunting by measuring the reverse bias leakage current in the dark. This value was comparable for cells on both ZnO and SnO_2. Then using the metal scribe process we scribed across several of the small area cells to divide each cell into two smaller cells. We then repeated the reverse bias current leakage measurement on the smaller cells. There was no change in the degree of shunting for cells on SnO_2 before and after the metal scribe. On the other hand, all the cells on ZnO showed higher leakages, suggesting that the metal

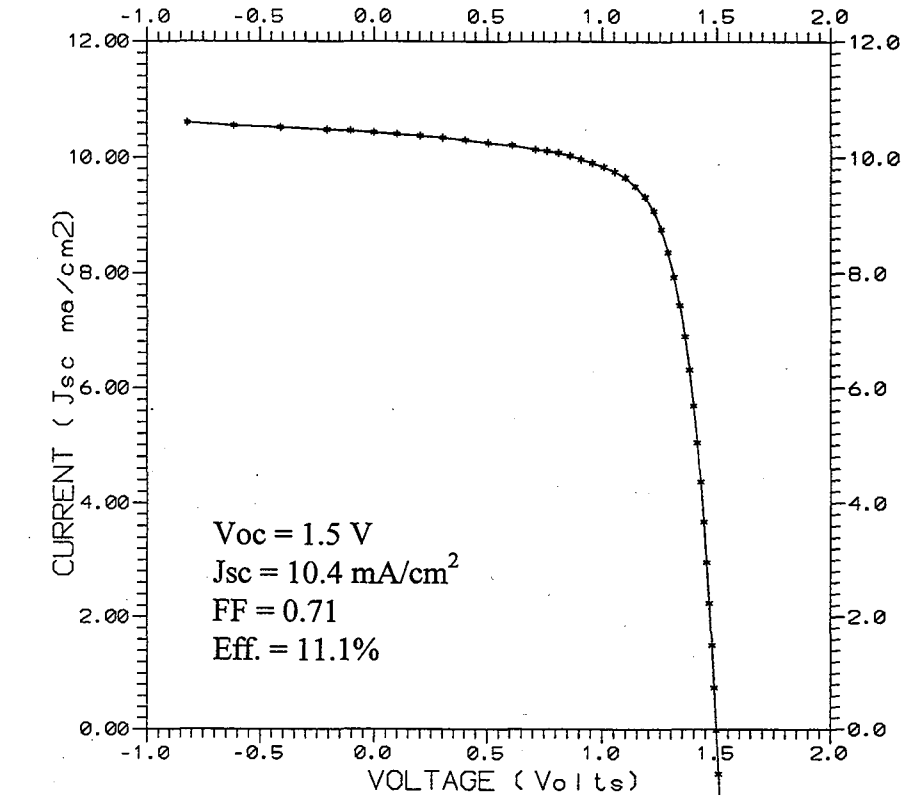

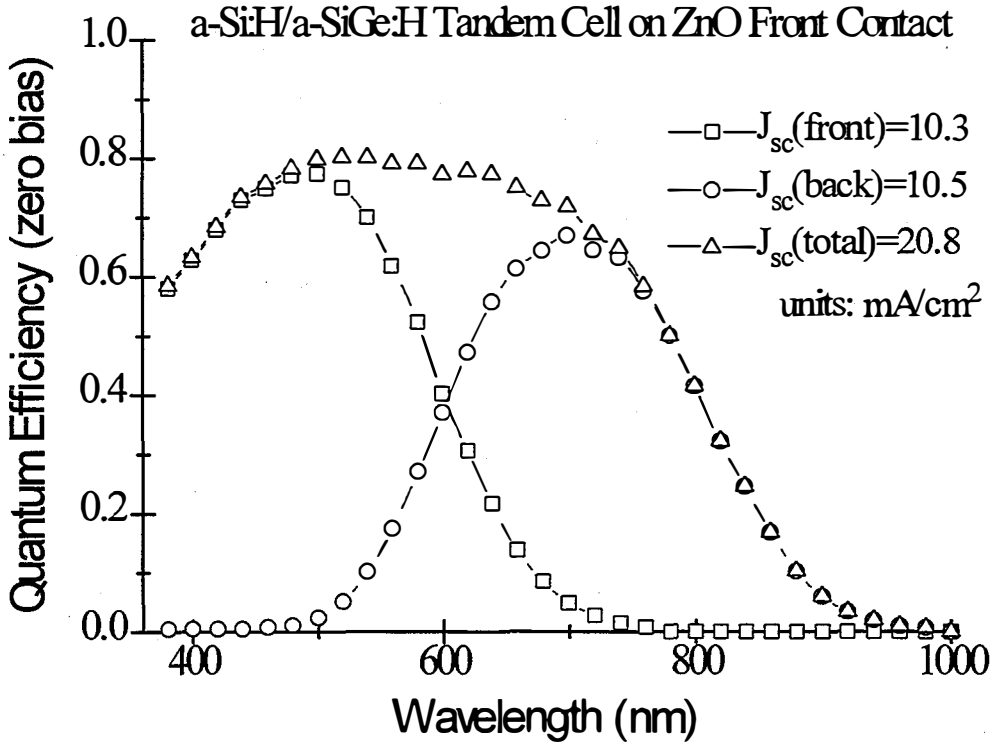

Figure 16 J-V curve and QE of a typical a-Si:H/a-SiGe:H tandem cell made on ZnO.

scribe process is creating a shunt path along the sides of the cells. We are currently optimizing the metal scribe process for ZnO modules.

3.2 Tunnel Junction

3.2.1 Test Structure for Tunnel Junction

It has been increasingly recognized that using a multijunction solar cell as a test device to assess the quality of the tunnel junction is inefficient and sometimes even ambiguous. Multijunction devices usually take much longer to deposit than single-junction devices. Furthermore, the electrical characteristics of the multijunction devices, especially the FF, are affected not only by those of component junctions, including the tunnel junction, but also by factors such as current balance among junctions. The relationship to all those factors are not completely understood, making it difficult to extract useful information about the tunnel junction itself. Therefore, it would be of great importance to develop a simpler test structure for tunnel junction by attaching it to an a-Si:H control p-i-n cell whose electrical characteristics are well established. The simpler test structure would hopefully make the tunnel junction optimization and scale-up processes much more efficient.

While the tunnel junction can in principle be attached to either the p- or the n- layer of the single-junction device, i.e. p-i-n-p or n-p-i-n, to form a test structure, the p-i-n-p device does not in reality make good contact to the ZnO/Al back contact. This is not surprising because ZnO is n-type and in our experience it requires special care to make good contact to the p-layer. On the other hand, there is no difficulty in making good ohmic contact between the SnO_2 front contact which is also n-type and the n-layer as part of the tunnel junction. Therefore, by using the n-p-i-n structure as the test device, any decrease in V_{oc} and FF can be simply attributed to the effect of the tunnel junction. The only correction in V_{oc} and FF in order to compare with its single-junction device counter part is the lower photocurrent effect due to absorption in the extra n-layer, which can be simulated by measuring the single junction device with an appropriate cut-on filter. To establish the usefulness of this test structure, we have purposely made tunnel junctions in both n-p-i-n and Si/Si tandem device structures with a large variation in the deposition condition. As shown in Table 5 where some of the device parameters are listed, there is good correlation in the performance of the two types of devices. Tunnel junction type A, B, C denote different conditions under which the tunnel junctions in the devices were made. Also listed in Table 5 is the parameters of the control Si single junction device with and without the cut-on filter.

3.2.2 Uniformity of Microcrystalline Tunnel Junction

Since the microcrystalline tunnel junction is deposited with extremely high H_2-dilution and high power, it is considered the most difficult component of the tandem device to be deposited uniformly over large area. To evaluate the uniformity of the tunnel junction, we have again taken advantage of the simple n-p-i-n test device. As compared to the full tandem device, the test structure has fewer layers so that the interpretation is much simpler because different layers

such as the microcrystalline tunnel junction and the a-SiGe:H i-layer may have different non-uniformity patterns.

Table 5 Comparison of n-p-i-n and Si/Si devices

Sample #	Device	Tunnel J.	V_{oc} (V)	J_{sc} (mA/cm^2)	FF	R_s (Ωcm^2)
MC5023-1	p-i-n control	No	0.94	13.6	0.69	5.3
	w/ cut-on filter		0.91	8.8	0.69	7.3
MC5027-3	n-p-i-n	type A	0.91	8.3	0.72	7.8
MC5024-3	Si/Si		1.83	7.0	0.71	17.5
MC5032-3	n-p-i-n	type B	0.89	8.9	0.63	23.2
MC5010-1	Si/Si		1.85	7.2	0.64	43.7
MC5047-2	n-p-i-n	type C	0.82	8.7	0.72	7.3
MC5053-4	Si/Si		1.71	6.7	0.70	19.1

We have deposited n-p-i-n devices with a typical microcrystalline tunnel junction on 12"x13" substrates which cover ~85% of the cathode area. The devices were subsequently laser isolated into 416 individual cells which were then systematically tested using an automatic tester. Figure 17 shows the uniformity maps of one such device, MC5080-3. The three device parameters listed, i.e. V_{oc}, FF and Rs (series resistance), are the most critical ones for evaluating tunnel junctions. As evident in Fig. 17, except for a few point defects which are shorted cells caused primarily by laser isolation, the uniformity of all three parameters is actually quite good. No significant edge effects are visible. However, it is noticeable that the device performance is slightly better in the lower right half of the substrate than in the upper left half. The difference in V_{oc} between the two halves is on the order of 1% and in FF it is about 3%.

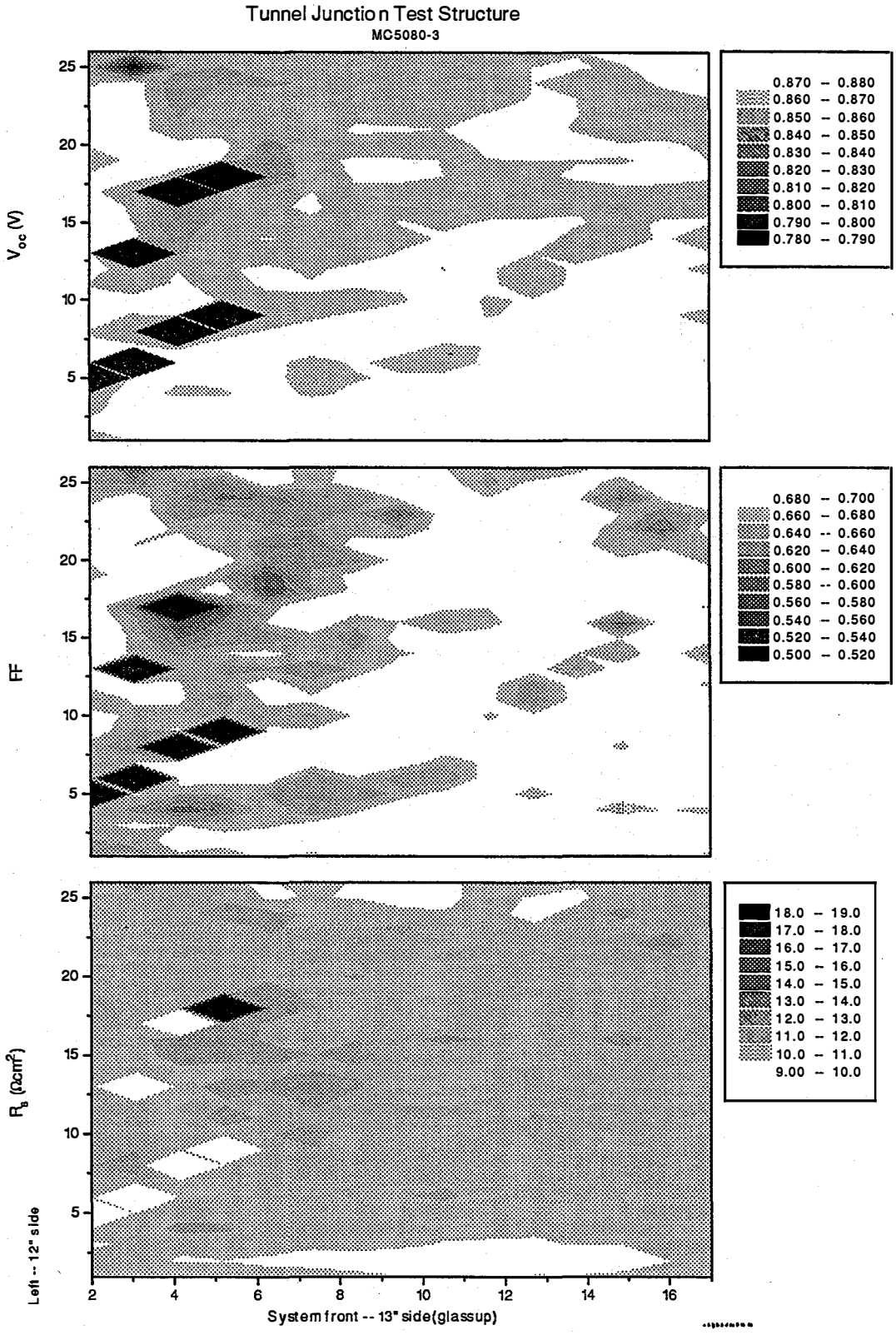

Figure 17 Uniformity of tunnel junction tested using n-p-i-n structure.

3.2.3 Tunnel Junction Optimization

The standard microcrystalline tunnel junction used in the multijunction devices consists of three to four individual doped layers and takes a minimum of four steps to deposit. Figure 18 is a schematic diagram of the standard tunnel junction. Its complicated structure and processing steps not only presents a problem for process control, but also makes it much harder to optimize. Therefore, it is extremely desirable to simplify the structure of the tunnel junction, for example, by eliminating the a-Si:H n-layer. To do this, it requires that the microcrystalline n-layer be directly nucleated from the intrinsic a-Si:H surface and maintains good electrical contact. We have done systematic experiments on eliminating the amorphous n-layer and optimizing the microcrystalline n-layer which is directly deposited on top of the i-layer. This new tunnel junction has helped in achieving higher FF on large area modules.

To further reduce optical loss in the tunnel junction, we have done an experiment to reduce as much as possible the thickness of the microcrystalline n-layer in the tunnel junction. Figure 19 shows the long wavelength (800 nm) quantum efficiency for tandem modules as a function of the microcrystalline n-layer thickness normalized to that of the standard process. It is apparent that the QE red response increases as the thickness of the tunnel junction decreases. Although in this set of experiments we did not adjust the current balance to take advantage of the current increase, the experiments did establish that thinning the tunnel junction by 33% does not cause any loss in V_{oc} and FF. However, as expected, significant further thickness reduction, e.g. by 50%, would lead to lower FF. Table 6 lists the module parameters.

Table 6 Module parameters with thinner tunnel junction

Module #	μc-N layer thickness reduction	V_{oc} (V)	FF (%)	J_{sc} (mA/cm^2)	Eff. (%)
H5231-3R	Standard	1.54	68.7	9.28	9.52
H5231-7R	33%	1.54	68.1	9.32	9.50
H5231-8R	50%	1.54	64.4	9.28	8.94

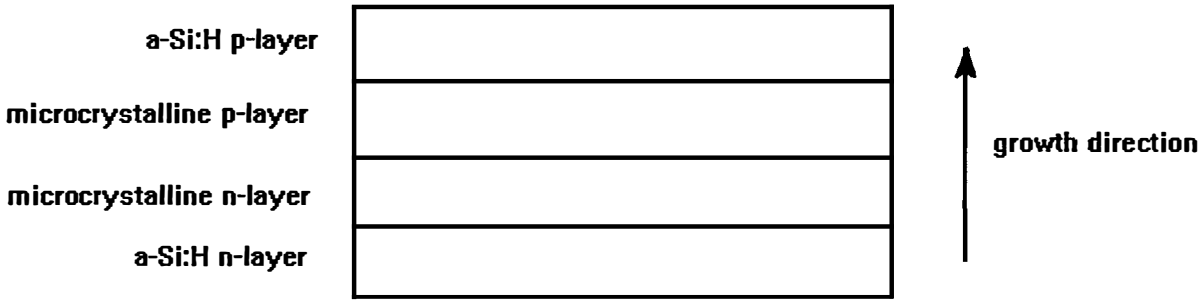

Figure 18 Schematic of tunnel junction used in tandem devices

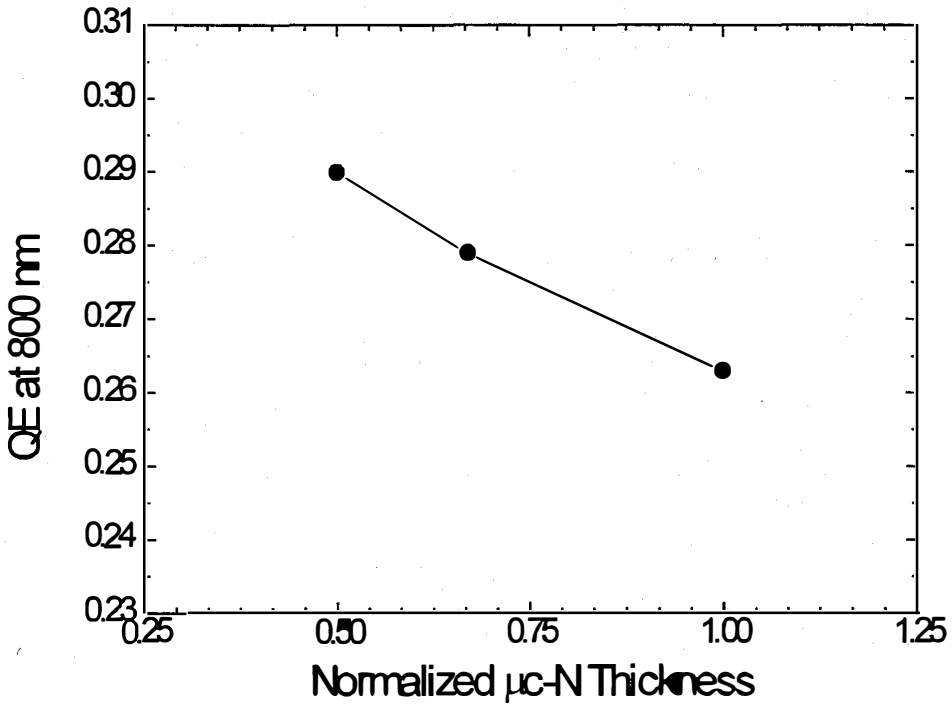

Figure 19 QE at 800 nm plotted versus microcrystalline n-layer thickness.

3.3 Composite Rear Contact

Previously, we observed that for a-Si/a-SiGe double-junction modules whose total thickness of a-Si layers is ~4000-5000 Å, the ZnO/Ag back contact did not work adequately due to excessive shunts which resulted in poor performance and low yield. Shunting was not as much an issue with the thicker triple-junction modules when the ZnO/Ag process was first developed. It has often been found that even for small area diodes, ZnO/Ag contact is more prone to shunting than the alternative ZnO/Al which is presently used as the back contact for our pilot-production 4 Ft^2 tandem modules. Unlike ZnO/Ag, ZnO/Al back contact not only tends to show less shunting, but the shunts are more likely to be curable. As shown earlier [3] and repeated here in Figures 20 & 21, there exist clear differences in shunting and efficiency between 1 Ft^2 tandem modules using ZnO/Ag and ZnO/Al as back contacts. These a-Si/a-SiGe modules were fabricated on the same type of SnO_2-coated glass using the same deposition recipe. In most instances, the ZnO/Ag contact led to so much shunting that any gain in J_{sc} is more than offset by the loss in FF (and V_{oc}) such that the module conversion efficiency would be lower than that obtained from the ZnO/Al back contact.

In order to take advantage of the higher reflectivity of ZnO/Ag and hence gain J_{sc} and efficiency without jeopardizing module yield due to shunting, we have explored ways to combine ZnO/Ag with other metal and/or metal-oxide layers to make composite back contacts, ZnO/Ag/X, where X is some "protective" layer or layers. In the ZnO/Ag/X configuration, a relatively thin layer of Ag (e.g., 500 Å) is sandwiched between ZnO and X. The idea is to make the ZnO/Ag behave like an extension of the a-Si:H *n*-layer as far as laser scribing and electrical curing are concerned. The "protective" layer (or layers) X must satisfy several conditions, such as being electrically conductive, shunt-resistant, and compatible with Ag in terms of adhesion and absence of inter-diffusion. Ideally, in the ZnO/Ag/X contact, the ZnO/Ag should dominate the optical but not the electrical behavior of the contact so as to minimize Ag-related shunting. The X layer(s) should facilitate electrical contact and help minimize shunts, both intrinsic and scribing-related. The preliminary data on module efficiency and shunting behavior are encouraging for the ZnO/Ag/X type back contact, where our proprietary choice of X (whose possibilities are quite numerous) is such that, when X itself is used alone as the back contact, there is little shunting for the modules. Compared to ZnO/Al, the ZnO/Ag/X composite back contact gives higher J_{sc} (~5%) according to QE measurements on small area cells, as exemplified by Fig. 22, mainly due to increased red response as expected from higher reflectivity of Ag over Al.

Higher conversion efficiencies have also been observed for 1 Ft^2 a-Si:H/a-SiGe:H tandem modules using the ZnO/Ag/X composite rear contact due mostly to higher FF presumably as a result of the favorable overbalance of J_{sc} of the a-SiGe:H back junction compared to the case of ZnO/Al. Figures 23 and 24 compare a dozen runs of co-deposited 1 Ft^2 a-Si/a-SiGe tandem modules with either standard ZnO/Al or the new ZnO/Ag/X composite back contact. Figure 23 shows significant gain in the absolute conversion efficiency when ZnO/Ag/X composite back contact is used instead of ZnO/Al. The efficiencies for the modules are all over 9% irrespective of the type of back contact. Figure 23 shows the relative percentage gain in FF of the above

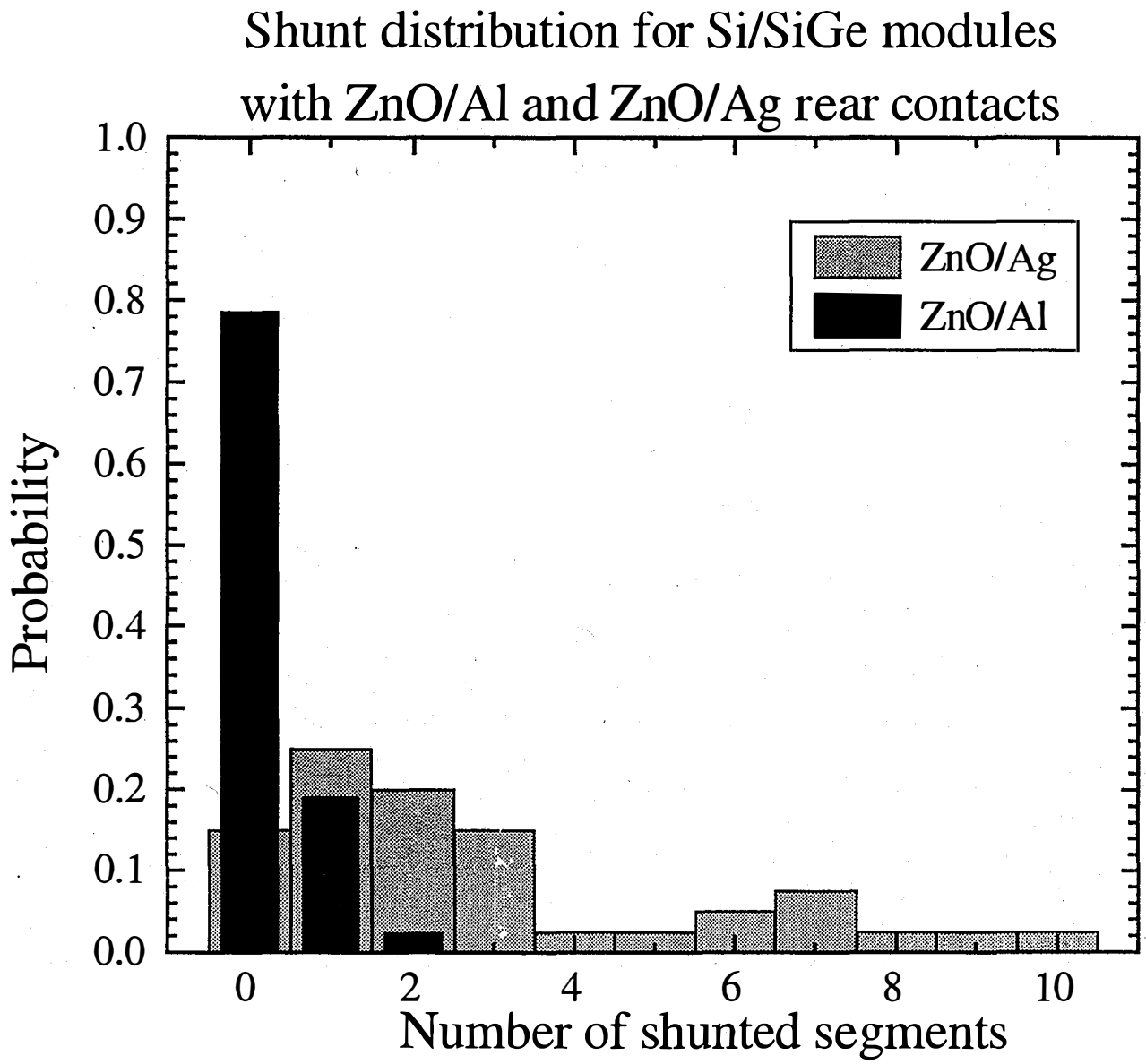

Fig. 20 Shunt distributions for 1 Ft^2 a-Si:H/a-SiGe:H tandem modules with ZnO/Al

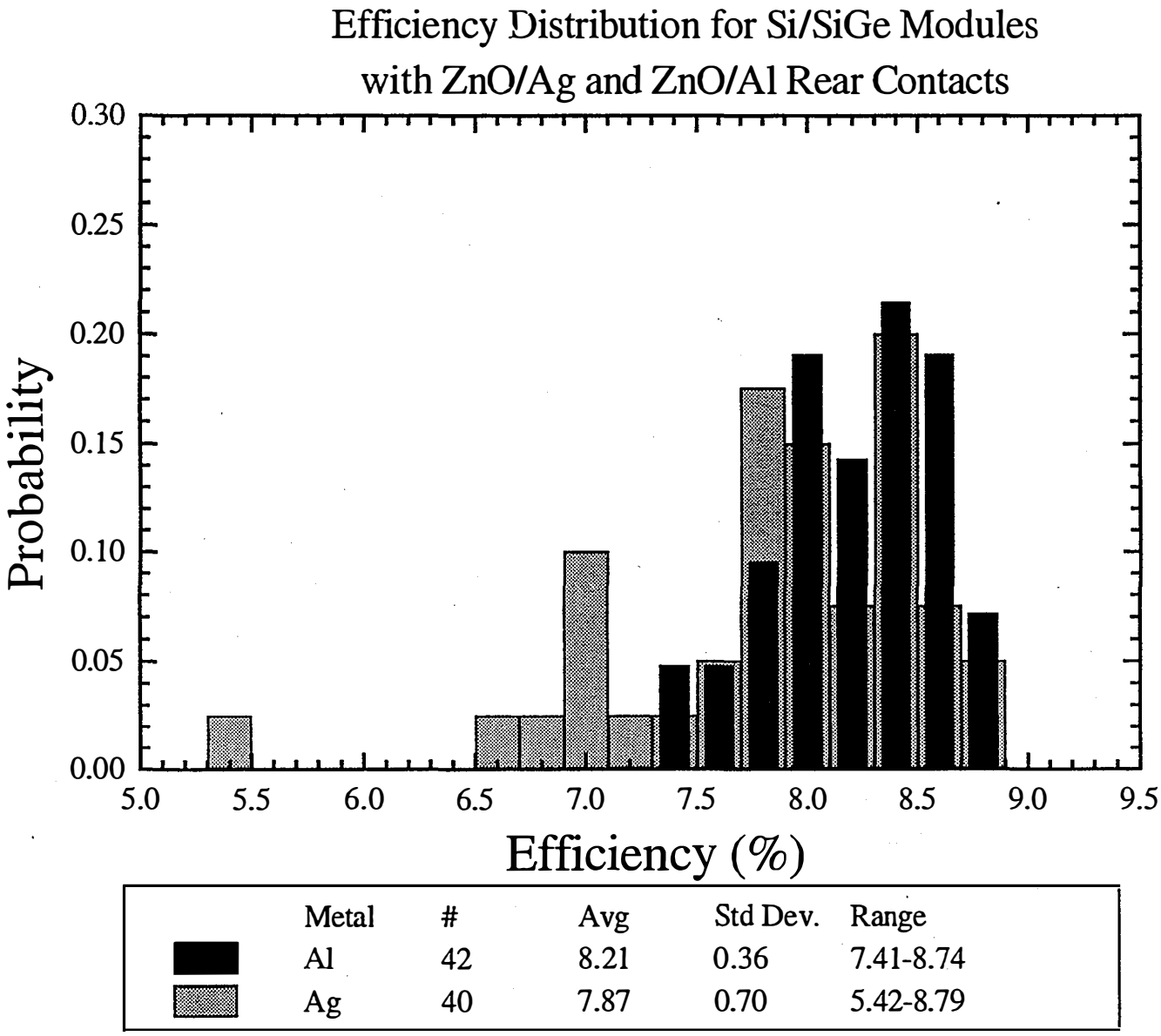

Fig. 21 Efficiency distribution for 1 Ft^2 a-Si:H/a-SiGe:H tandem modules with ZnO/Al and ZnO/Ag rear contacts.

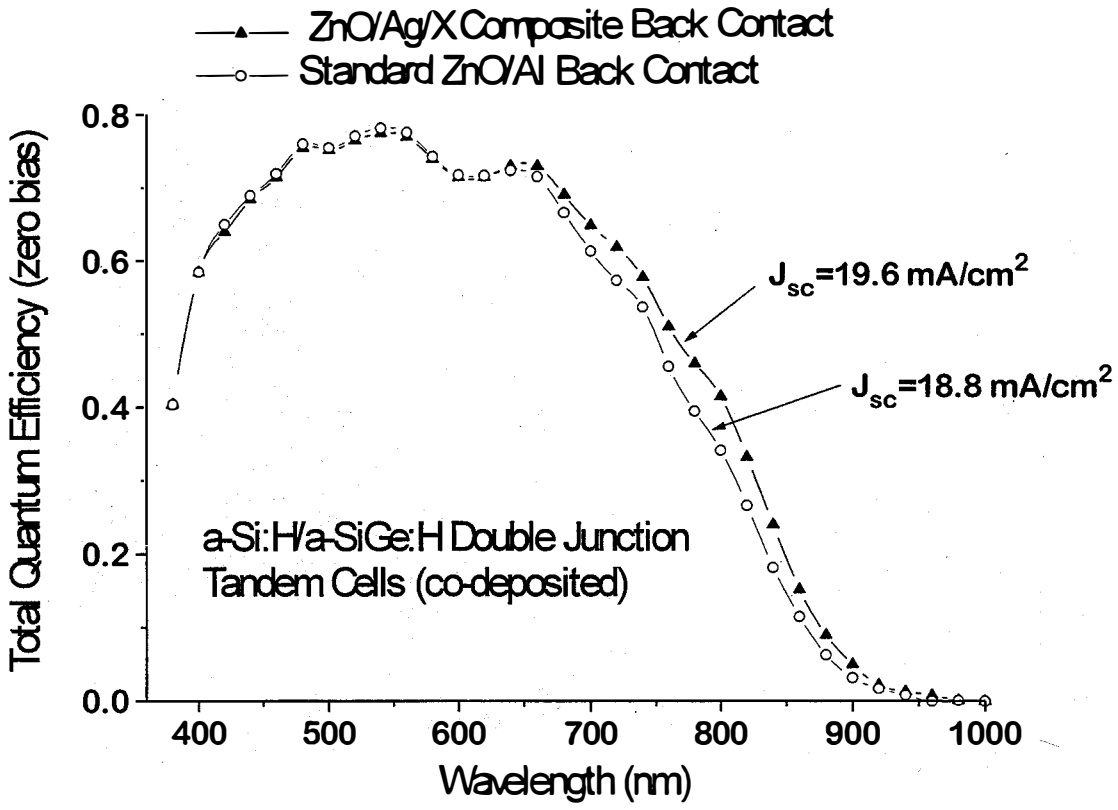

Figure 22 Comparison of total QE spectra of co-deposited a-Si:H/a-SiGe:H tandem cells (0.26 cm^2) with standard ZnO/Al back contact and with ZnO/Ag/X composite back contact.

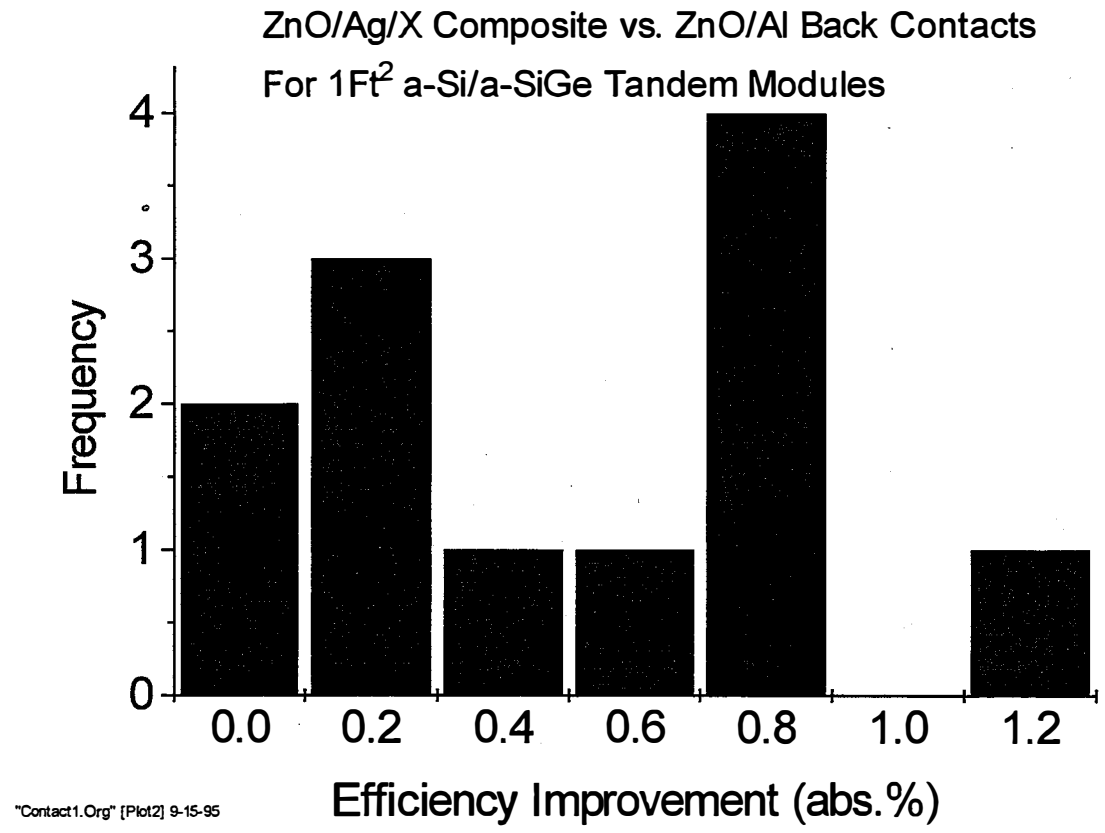

Figure 23 Distribution of efficiency improvement of 1 Ft^2 a-Si:H/a-SiGe:H tandem modules with the new ZnO/Ag/X composite contact compared to identically deposited modules with the standard ZnO/Al rear contact.

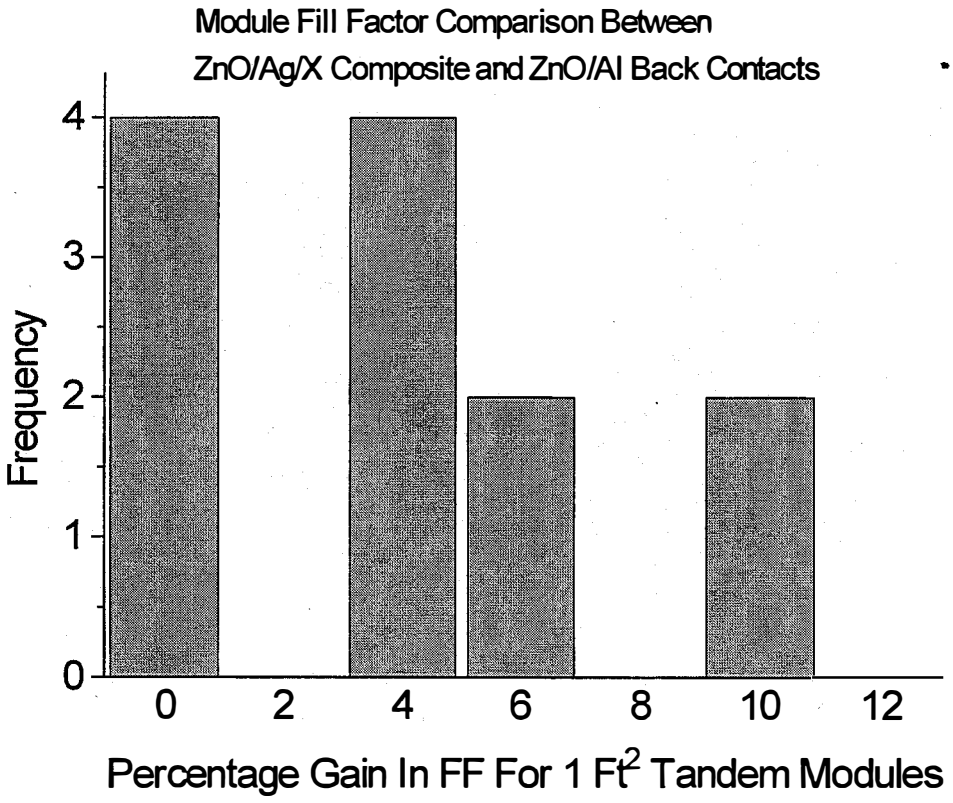

Figure 24 FF improvement distribution of 1 Ft^2 tandem modules by using the ZnO/Ag/X composite rear contact in comparison with the standard ZnO/Al rear contact.

modules by using the new ZnO/Ag/X composite back contact in comparison with the co-deposited modules with ZnO/Al back contact. We are in the process of collecting more of such comparative data. Note that, there has been no significant difference in module J_{sc} between the two types of contacts (within ~0.1 mA/cm^2), as the current is well balanced between the front and back junctions when ZnO/Al is used.

More importantly, compared to the simple ZnO/Ag contact (where the Ag thickness is ~200 nm), the module shunting problem is much less severe when ZnO/Ag/X composite back contact is used, as illustrated in Fig. 25. Most of the modules with ZnO/Ag/X contact show either no shunting or very mild shunting, unlike the ZnO/Ag case shown in Fig. 20. Although the ZnO/Ag/X composite contact still shows tendency toward shunting than ZnO/Al, the problem is much less severe compared to the conventional ZnO/Ag contact. Thus the ZnO/Ag/X composite contact is promising as a potentially manufacturable process as far as module yield is concerned. It is interesting to note that, even for the improved ZnO/Ag/X back contact, the likelihood of module shunting increases greatly with the delay time between a-Si:H deposition and the contact (ZnO) deposition. In contrast, the module shunting behavior of ZnO/Al contact is far less sensitive to such time delay, although the electrical properties (FF and series resistance) do degrade with delay. In general, particles and debris on the module cause shunting problems for any type of contact.

We are conducting more experiments on this new type of back contact, both in terms of recipe variation and module processing compatibility (such as laser scribing procedure). Further and in particular, we are going to evaluate the long-term stability of the ZnO/Ag based composite contact, since previously we saw some evidence that the conventional ZnO/Ag showed notable degradation compared to ZnO/Al, so that after prolonged light exposure, the initial difference in J_{sc} (~4-6%) would become negligible due to apparent "tarnishing" of the ZnO/Ag interface.

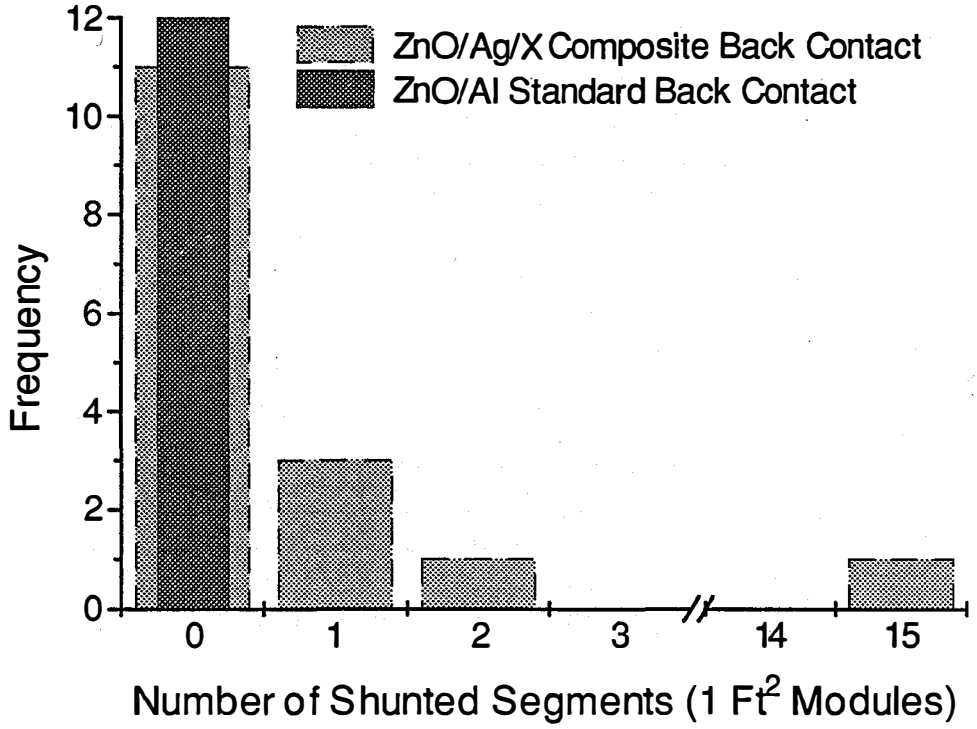

Figure 25 Shunt distributions for 1 Ft^2 tandem modules with ZnO/Al or ZnO/Ag/X rear contact.

3.4 Low-temperature Devices

The standard a-Si:H/a-SiGe:H tandem structure used in our pilot production is made at a constant substrate temperature throughout the entire semiconductor deposition process. We have demonstrated earlier that further lowering deposition temperature and increasing H_2 dilution can significantly increase the open circuit voltage of a-Si:H single junction cell and at the same time improve its stability against light soaking [15]. However, depositing a-SiGe cells at lower temperatures was found to be difficult in our earlier attempts. Therefore, we have investigated the feasibility of depositing two junctions in a tandem device at different temperatures using a multi-chamber system.

The three deposition chambers in the multi-chamber system used to be configured as dedicated p, i, and n chambers for the purpose of isolating dopants from the intrinsic material. Now we have re-configured the system to do low temperature a-Si:H intrinsic material as well as all n-layers in the old n-chamber.

Since the low temperature front junction will be exposed to higher temperature for at least the duration of the second junction deposition, it is necessary that the low temperature devices do not lose open circuit voltage after post deposition annealing. To test this we have made a single junction Si device at low temperature and then annealed the sample in vacuum at the standard temperature for 30 min. The comparison of this device with that made under the same condition except without the last annealing step is shown in Table 7. It is clear that no loss of V_{oc} has occurred due to the post annealing step.

Table 7 Low temperature a-Si:H devices made with and without post annealing

Sample #	Post-annealing	V_{oc} (V)	FF (%)	J_{sc} (mA/cm2)	Eff. (%)
MC4341-4	No	0.953	71.3	12.11	8.23
MC5012-4	Yes	0.973	68.1	12.05	7.98

We have tested the concept of hybrid tandem cells by making Si/Si devices with front junction i-layers made at low temperature and back junction i-layers made at regular temperature. The device parameters are listed in Table 8 together with the cell in which both i-layers were made at the regular temperature. A substantial gain in V_{oc} (~30 mV) was observed for the device with low temperature i_1-layer which is consistent with that observed in single junction devices. This result further confirms that higher V_{oc} from the low temperature front junction can be preserved even if the second junction of the tandem device is deposited at a substantially higher temperature. Now that we have obtained all necessary proof-of-concept, we have begun to make the actual a-Si:H/a-SiGe:H tandem device incorporating the low temperature i_1-layer.

Table 8 Si/Si tandem cells with and without low temperature front i-layer

Sample #	Low T I_1-layer	V_{oc} (V)	FF (%)	J_{sc} (mA/cm2)	Rs (Ω cm2)	Eff. (%)
MC5032-4	Yes	1.860	69.8	7.17	18.7	9.31
MC5024-3	No	1.832	71.4	6.99	17.5	9.14

3.5 Tandem Modules

3.5.1 Performance

Module development involves scale-up of various thin-film processes, such as, the textured tin oxide front contact, the amorphous silicon based alloys and the zinc oxide/aluminum rear contact to 1 ft^2 and optimization of segment width and laser scribing to minimize sheet-resistance and inter-connect losses. The tandem junction device structure that we have pursued for this purpose is shown in Figure 26.

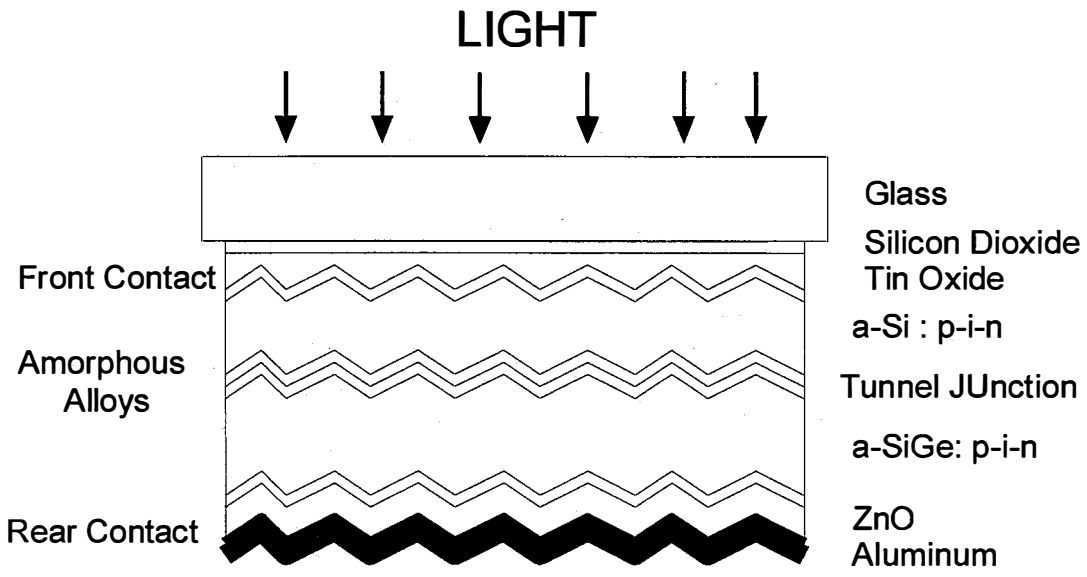

Figure 26 Device structure for tandem junction a-Si/a-SiGe modules.

The best module fabricated with this device structure had an initial conversion efficiency of 10.46% as measured by NREL. The photovoltaic parameters of this module are tabulated in Table 9.

Table 9 Initial photovoltaic parameters of best 1 ft^2 tandem module

Module #	Aperture Area (cm^2)	V_{oc} (V)	I_{sc} (mA/cm^2)	F.F	Initial Efficiency(%)
H5238-3R	904.8	50.35	269.7	0.692	10.46

In module fabrication, more emphasis has been on process reproducibility and process control to demonstrate the statistical distribution of module fabrication processes.

Figure 27 shows a histogram of initial conversion efficiency of a batch of 76 modules produced by the same deposition processes (tin oxide, silicon, ZnO and Al) over a period of time. The average initial efficiency (as measured at Solarex) is 9.11% with a standard deviation of +- 0.39. The histograms for J_{sc}, V_{oc} and FF for these modules are shown in Figure 28.

We have established a systematic difference in indoor measurements made at Solarex and at NREL. On the average, the conversion efficiency measured at NREL is about 5.5% higher than that measured at Solarex. Table 10 shows the difference in measurements made at NREL and those made at Solarex on the same 1 ft^2 tandem junction modules.

Table 10 1 ft^2 tandem junction modules measured at NREL and at Solarex

Module #	**Aperture Area (cm^2)**	**V_{oc} (V)**	**I_{sc} (mA)**	**FF**	**Efficiency Aperture area matched to SLX**	**P_{max} (W)**	**Measured At**	**Delta in Efficiency**
H5231-5L	904.8	48.20	257.7	0.631	9.00	7.837	NREL	
	870.4				8.48	7.38	SOLAREX	6.13%
H5238-3R	904.8	50.35	269.7	0.692	10.46	9.395	NREL	
	897.6				9.95	8.93	SOLAREX	5.12%
H5245-5R	904.8	50.93	267.3	0.665	10.09	9.057	NREL	
	897.6				9.61	8.63	SOLAREX	4.99%
H5248-8M	904.8	50.49	271.1	0.669	10.23	9.18	NREL	
	897.6				9.68	8.69	SOLAREX	5.68%
H5252-4L	904.8	50.66	273.6	0.669	10.32	9.269	NREL	
	897.6				9.79	8.79	SOLAREX	5.41%
								Ave. 5.5%

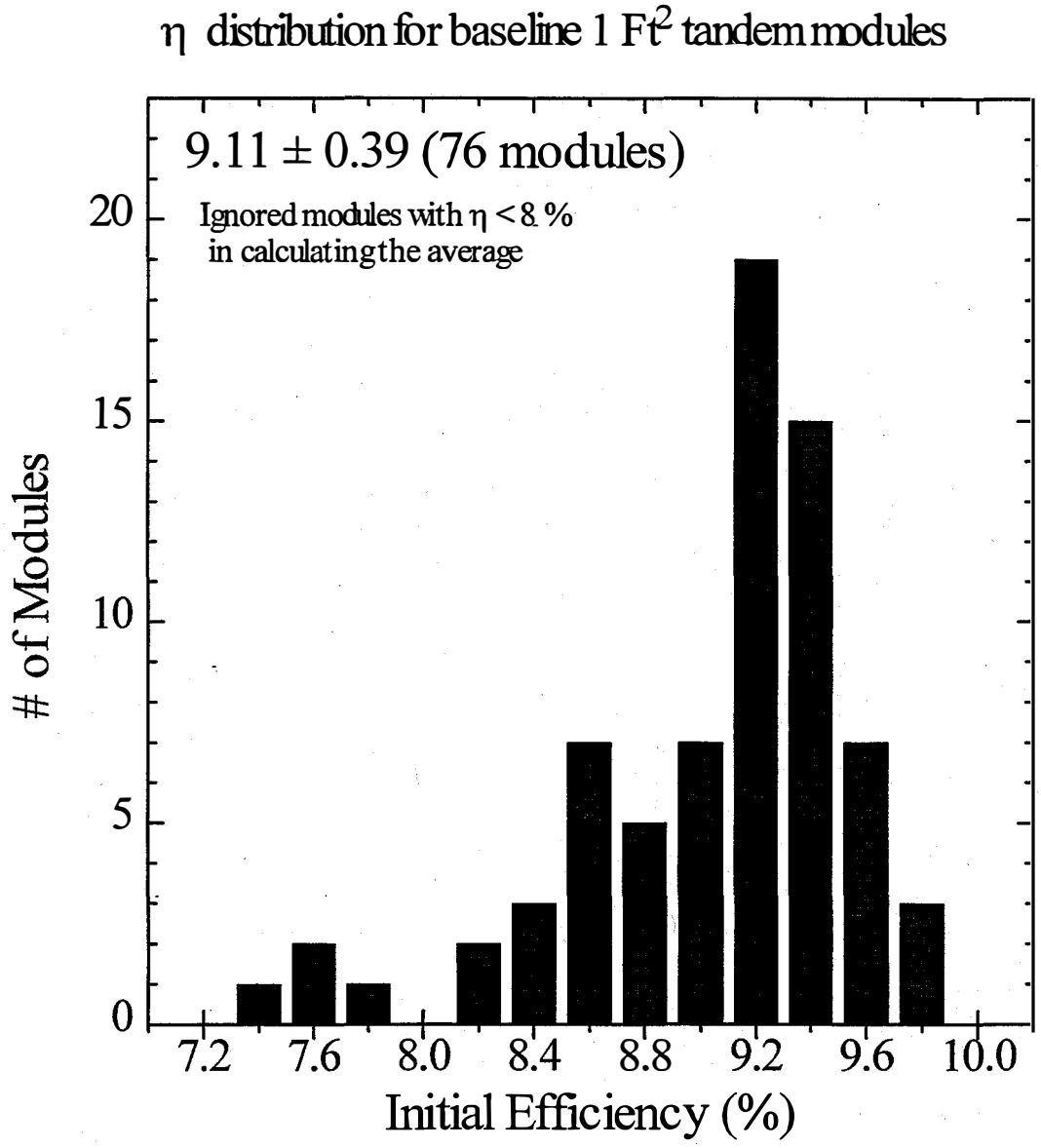

Figure 27 Initial conversion efficiency of 1 ft^2 tandem modules.

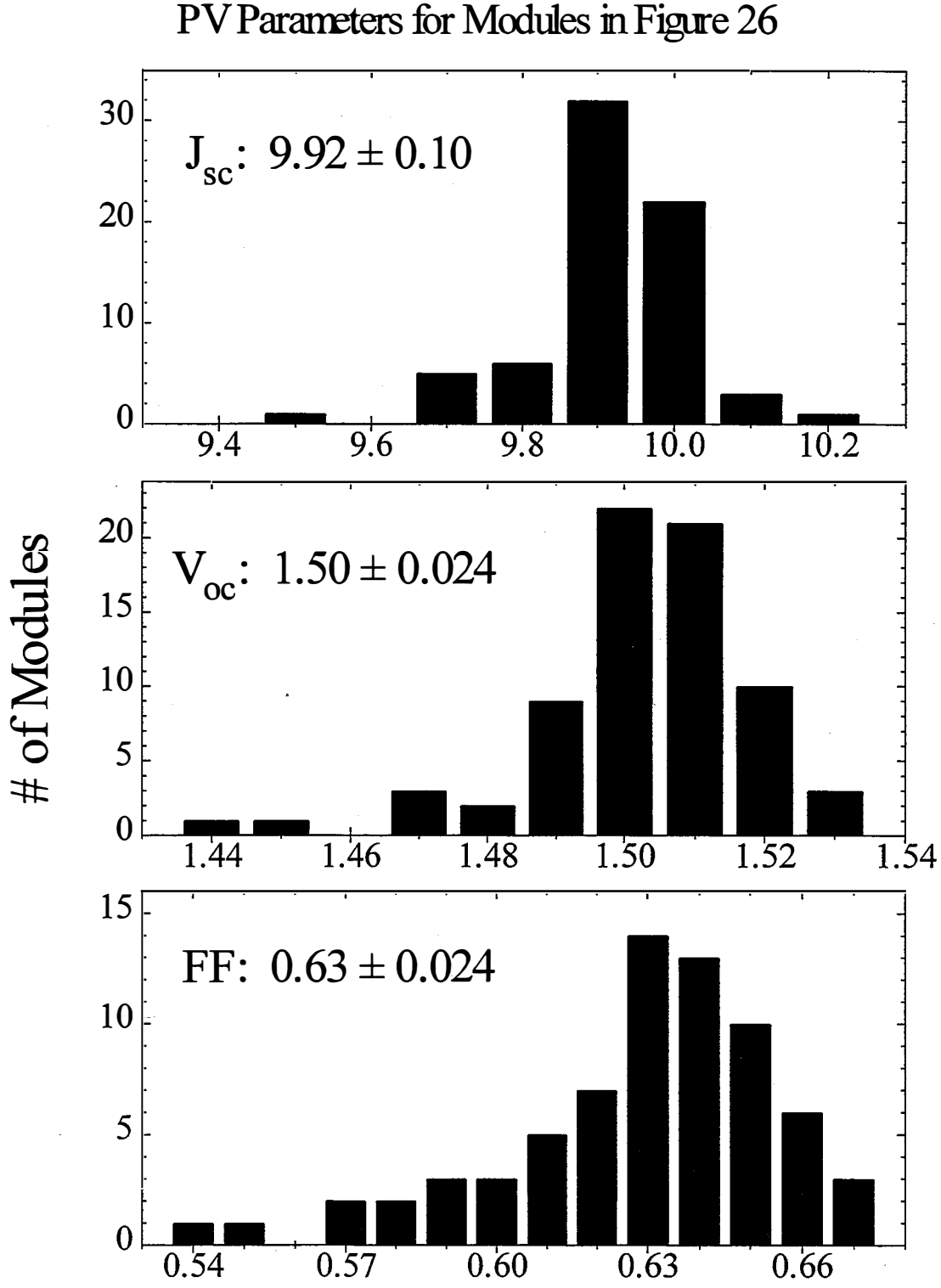

Figure 28 Photovoltaic parameters of modules in Figure 27.

3.5.2 Indoor Stability

The standard device structure shown in Figure 25 consists of an a-Si:H front junction and an a-SiGe:H back junction. The lowest bandgap in the graded bandgap back junction has a bandgap ~ 1.45 eV. The thicknesses of the two junctions are such that the total current density generated is about 20 mA/cm^2. Dozens of such 1 ft^2 and 4 ft^2 modules have been degraded by indoor light soaking using Na+ vapor lamps with intensity adjusted to AM1.5 and module temperature maintained at about 40°C. The average normalized module efficiency as a function of light soaking time is plotted in Fig. 28. After 600 hours of light-soaking, this device structure has exhibited an average degradation of ~17% which is certainly better than that of single-junction devices and, in our experience, is even comparable to that of a Si/Si/SiGe triple-junction device. Our light-soaking data was confirmed at NREL where two modules were light-soked for 800 hours. The initial and stabilized data is tabulated in Table 11.

Table 11 NREL Indoor Light Soaking results on tandem modules

Module #	Light Soak (hours)	V_{oc} / seg (V)	J_{sc} (ma/cm^2)	FF(%)	Efficiency (%)	Degradation (%)
H4301-3R	0	1.52	9.83	64.9	9.83	
	800	1.49	9.54	57.2	8.14	17.2
H4301-5R	0	1.52	9.83	64.4	9.75	
	800	1.50	9.54	56.7	8.12	16.8

3.5.3 Outdoor Stability

We have been testing our a-Si/a-SiGe tandem modules outdoors. Figure 29 shows the outdoor degradation of two 4 ft^2 modules with the same silicon process as shown in Figure 26. The modules degrade between 16%-18% after more than 200 days of outdoor exposure. We have set-up a 1 kW array of 4 ft^2 modules at NREL. Initial results from outdoor testing at NREL show a degradation of 10.9% in conversion efficiency after 75 days, a very encouraging result.

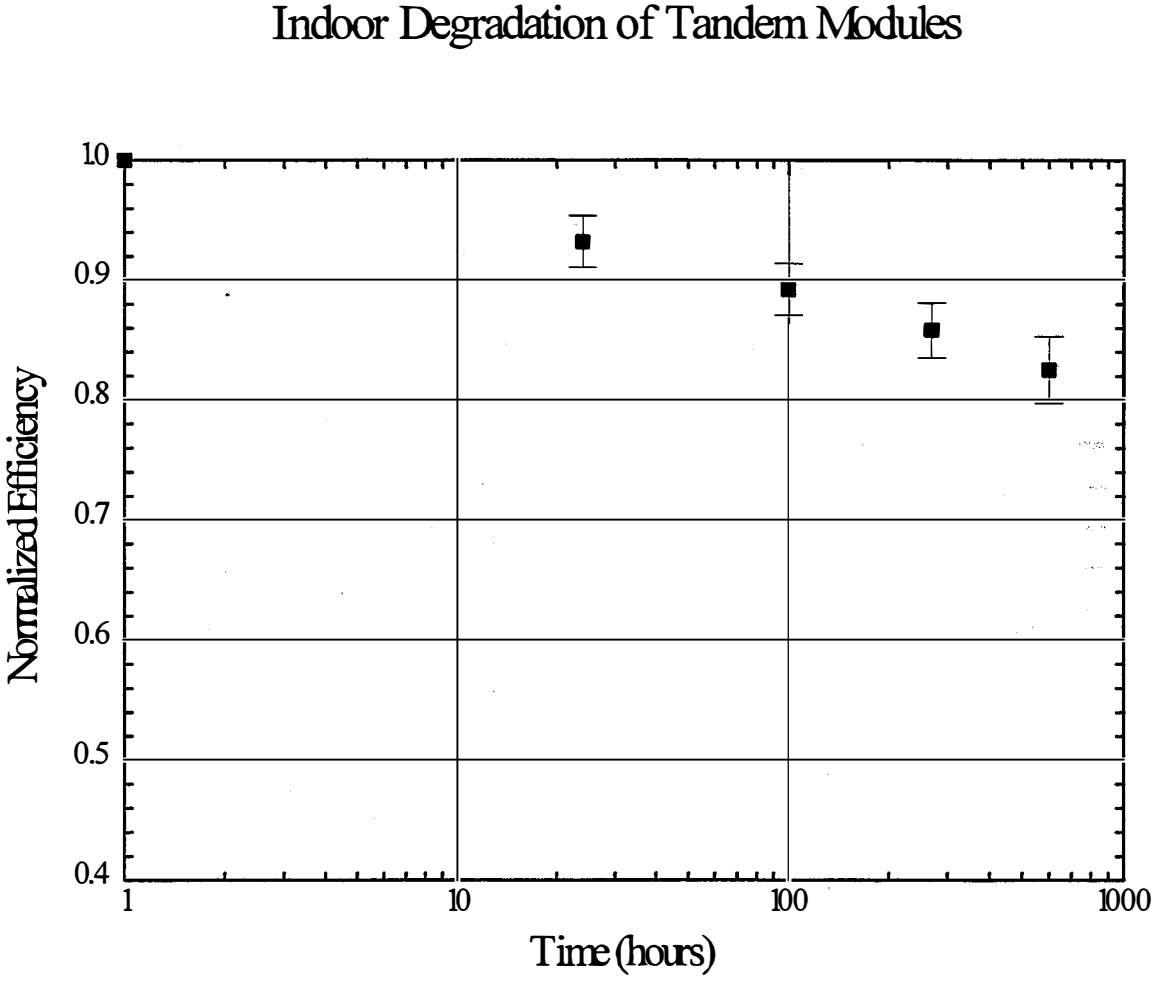

Figure 28 Indoor degradation of a-Si:H/a-SiGe:H tandem modules. The average normalized module efficiency with error bar is plotted versus light soaking time.

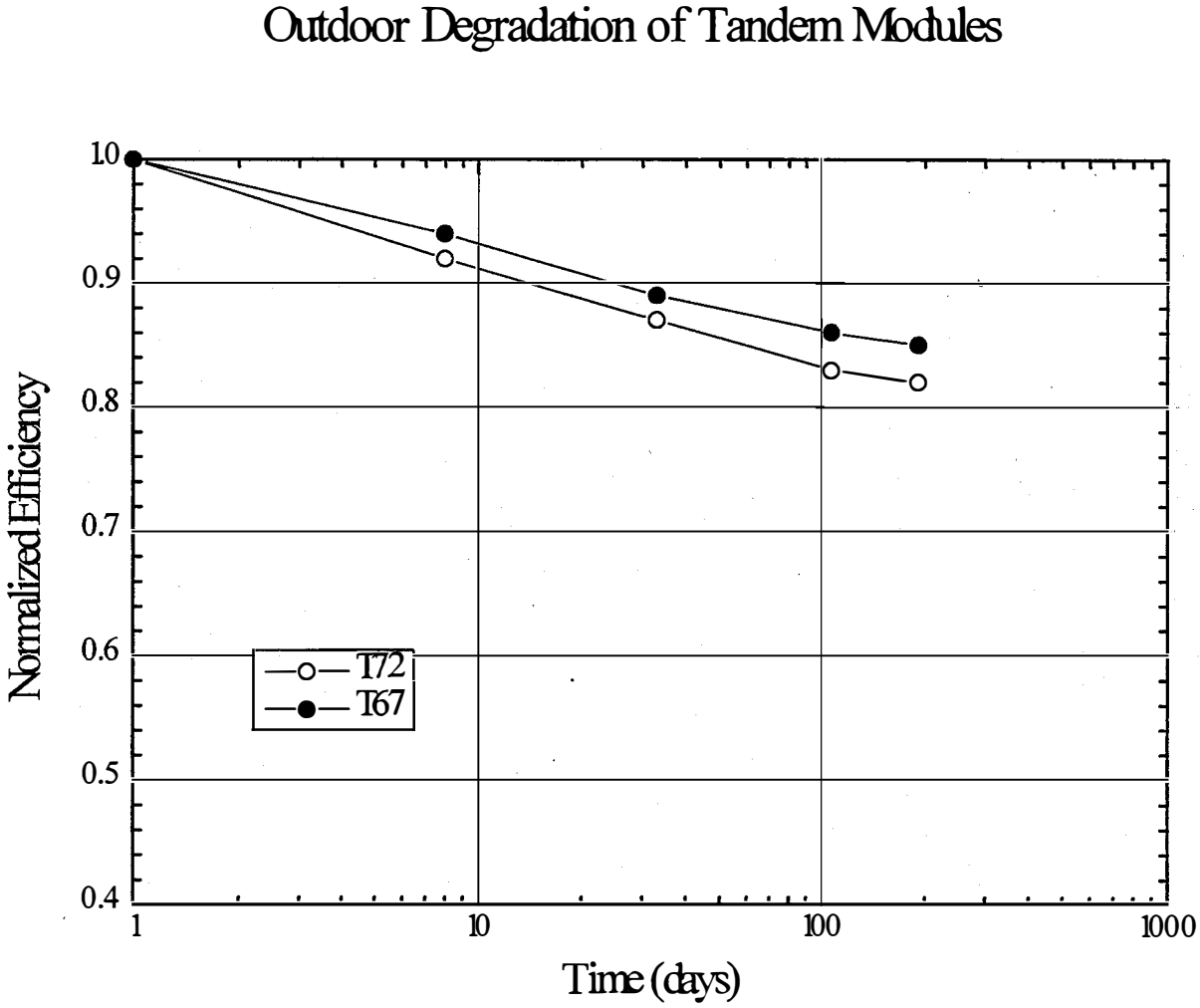

Figure 29 Outdoor degradation of two 4 ft^2 a-Si:H/a-SiGe:H tandem modules. The normalized module efficiency is plotted versus days of outdoor exposure at Newtown, PA.

3.6 Module Status and Future Directions

During the first year of the research contract significant improvements have been made in the area of a-Si:H front junction and the overall performance of the rear contact. A robust manufacturable a-Si/a-SiGe tandem process was developed which has an average initial efficiency of ~ 9.6% and an average stabilized efficiency of ~8% on modules with size up to 4 ft^2. The best 1 ft^2 module with this device structure had an initial efficiency of 10.5% and a stabilized efficiency of 8.7%.

During the next two years of the contract efforts will be concentrated towards incorporation of ZnO as the front contact which should increase the conversion efficiency by 7%, improvements in a-SiGe:H alloys and improvements in reflection from the rear contact should also increase the efficiency by 7%, resulting in stabilized performance above 9% with a manufacturable process. Several elements of the a-Si/a-SiGe tandem process which either increase a-Si alloy deposition thruput or reduce material usage's and reduce process variation will also be incorporated to demonstrate a cost-effective tandem process.

REFERENCES

[1] M. Bennett, K. Rajan and K. Kritikson, in *Conf. Recond of the 23rd IEEE Photovoltaic Specialist Conf.* (Louisville, KY, 1993) p. 790.

[2] R. Arya et al., in *Conf. Recond of the 23rd IEEE Photovoltaic Specialist Conf.* (Louisville, KY, 1993) p. 790.

[3] R. Arya et al., in *Conf. Recond of the 1st World Conf. On Photocoltaic Energy Conversion* (Waikoloa, Hawaii) p.394

[4] Y. Ichikawa et al., in *Conf. Recond of the 23rd IEEE Photovoltaic Specialist Conf.* (Louisville, KY, 1993) p. 27.

[5] F. Willing, M. Bennett and J. Newton, Proc. 19th IEEE Photovoltaic Specialists Conf., IEEE, N.Y. (1987). p. 1086.

[6] R. R. Arya, R. S. Oswald, Y. M. Li, N. Maley, K. Jansen, L. Yang, L. F. Chen, F. Willing, M. S. Bennett, J. Morris and D. E. Carlson, First World Conference on Photovoltaic Energy Conversion, Waikoloa, Hawaii, Dec. 5-9, 1994.

[7] D. E. Carlson, R. R. Arya, M. Bennett, L.- F. Chen, K. Jansen, Y.- M. Li, N. Maley, J. Morris, J. Newton, R. S. Oswald, K. Rajan, D. Vezzetti, F. Willing and L. Yang, AIP Conf. Proc. 353 (AIP, New York, 1995).

[8] D. L. Staebler and C. R. Wronski, Appl. Phys. Lett. **31**, 292 (1977).

[9] D. E. Carlson and C. W. Magee, Appl. Phys. Lett. **33**, 81 (1978).

[10] P. V. Santos, N. M. Johnson and R. A. Street, Phys. Rev. Lett. **67**, 2686 (1991).

[11] W. Beyer, J. Herion and H. Wagner, J. Non-Cryst. Solids **114**, 217 (1989).

[12] P. V. Santos, N. M. Johnson and R. A. Street, Phys. Rev. Lett. **67**, 2686 (1991).

[13] P. V. Santos, J. Phys: Condensed Matter **5**, A335 (1993).

[14] L. Yang and L. Chen, *Appl. Phys. Lett.* **63**, 400 (1993).

[15] L. Yang and L. Chen, MRS Symp. Proc. Vol. **336**, p. 669.

[16] Keda Wang, Daxing Han, and M. Silver, in "Amorphous Silicon Technology," edited by E. A. Schiff, M.Hack, A. Madan, M. Powell, A. Matsuda, (*MRS Symp.* Proc. **336** 1994) pp.861-866.

[17] Keda Wang and Daxing Han, in "Amorphous Silicon Technology" *MRS Symp.* (1995), in press.

[18] Daxing Han and Keda Wang, to be published in *J. Non-Cryst. Sol.* (1995).

[19] H. M. Branz and E. A. Schiff, *Phys. Rev* B **48** 8667 (1993).

[20] G. Lucovsky and S. Y. Lin, in "Optical Effects in Amorphous Semiconductors" edited by P.C. Taylor and S.G. Bishop, *AIP Proc.* **120** (1984) p.55.

REPORT DOCUMENTATION PAGE

Form Approved
OMB NO. 0704-0188

1. AGENCY USE ONLY (Leave blank)	2. REPORT DATE	3. REPORT TYPE AND DATES COVERED
	February 1996	Annual Subcontract Report, 1 October 1994 - 30 September 1995

4. TITLE AND SUBTITLE

Amorphous Silicon Research

5. FUNDING NUMBERS

C: ZAN-4-13318-01

TA: PV631101

6. AUTHOR(S)

R. R. Arya, M. Bennett, D. Bradley, L. Chen, K. Jansen, Y. Li, N. Maley, J. Newton, C. Poplawski, K. Rajan, L. Yang

7. PERFORMING ORGANIZATION NAME(S) AND ADDRESS(ES)

Solarex, A Business Unit of Amoco/Enron Solar
826 Newtown-Yardley Road
Newtown, PA 18940

8. PERFORMING ORGANIZATION REPORT NUMBER

9. SPONSORING/MONITORING AGENCY NAME(S) AND ADDRESS(ES)

National Renewable Energy Laboratory
1617 Cole Blvd.
Golden, CO 80401-3393

10. SPONSORING/MONITORING AGENCY REPORT NUMBER

TP-411-20708

DE96000526

11. SUPPLEMENTARY NOTES

NREL Technical Monitor: W. Luft

12a. DISTRIBUTION/AVAILABILITY STATEMENT

12b. DISTRIBUTION CODE

UC-1262

13. ABSTRACT *(Maximum 200 words)*

This report describes the research performed during the first year of a 3-year contract from NREL to accelerate commercialization of low-cost, high-performance, amorphous-silicon-based multijunction modules. Major accomplishments include (1) the development of a low-cost manufacturable a-Si/a-SiGe tandem junction process with average initial efficiency of 9.6% and average stabilized efficiency of 8%, (2) the demonstration of reduced degradation of tandem modules from ~17% to ~15%, (3) the optimization of hydrogen-diluted i-layer deposition and the development of a two-step i-layer that retains the stability advantages of H-dilution while decreasing the overall deposition time, (4) the development of an improved p-layer made with low growth rate and H_2 dilution.

14. SUBJECT TERMS

amorphous silicon ; photovoltaics ; solar cells ; multijuction modules ; stability ; hydrogen dilution

15. NUMBER OF PAGES
61

16. PRICE CODE

17. SECURITY CLASSIFICATION OF REPORT	18. SECURITY CLASSIFICATION OF THIS PAGE	19. SECURITY CLASSIFICATION OF ABSTRACT	20. LIMITATION OF ABSTRACT
Unclassified	Unclassified	Unclassified	UL